

# Lattice QCD study of the $s$ -wave $\pi\pi$ scattering lengths in the $I = 0$ and 2 channels

Ziwen Fu<sup>1,\*</sup>

<sup>1</sup> Key Laboratory for Radiation Physics and Technology of Education Ministry; Institute of Nuclear Science and Technology, College of Physical Science and Technology, Sichuan University, Chengdu 610064, People's Republic of China

(Dated: June 18, 2021)

The  $s$ -wave pion-pion ( $\pi\pi$ ) scattering lengths are computed below the inelastic threshold by the Lüscher technique with pion masses ranging from 240 MeV to 463 MeV. In the Asqtad-improved staggered fermion formulation, we calculate the  $\pi\pi$  four-point functions for the  $I = 0$  and 2 channels with “moving” wall sources without gauge fixing, and analyze them at the next-to-leading order in the continuum three-flavor chiral perturbation theory. At the physical pion mass, we secure the  $s$ -wave  $\pi\pi$  scattering lengths as  $m_\pi a_{\pi\pi}^{I=0} = 0.214(4)(7)$  and  $m_\pi a_{\pi\pi}^{I=2} = -0.04430(25)(40)$  for the  $I = 0$  and 2 channels, respectively, where the first uncertainties are statistical and second ones are our estimates of several systematic effects. Our lattice results for the  $s$ -wave  $\pi\pi$  scattering lengths are in well accordance with available experimental reports and theoretical forecasts at low momentum. A basic ingredient in our study for the  $I = 0$  case is properly incorporating disconnected diagram. These lattice computations are carried out with the MILC 2 + 1 flavor gauge configurations at two lattice spacings  $a \approx 0.15$  and 0.12 fm.

PACS numbers: 12.38.Gc, 11.15.Ha

## I. INTRODUCTION

The research on the  $\pi\pi$  scattering is a basic and classical subject in the field of strong hadronic interactions. Its handleability and simplicity essentially stem from the pseudo Nambu-Goldstone boson nature of pion, a natural aftermath of the spontaneous chiral symmetry breaking in quantum chromodynamics (QCD), which imposes rigid constraints on the  $\pi\pi$  low-energy interactions. Moreover, the  $s$ -wave  $\pi\pi$  scattering lengths vanish in the chiral limit when the momentum of the pions approaches zero. Since these quantities stand for a sensitive probe of the chiral symmetry breaking generated by the quark masses, the lattice QCD study, an objective of this paper, is a non-perturbative method in an effort to comprehend the low-energy nature of QCD.

With small pion masses and low-momenta, the  $s$ -wave  $\pi\pi$  scattering lengths can be solely predicted at leading order (LO) in chiral perturbation theory ( $\chi$ PT) [1]. The next-to-leading order (NLO) and next-to-next-to-leading order (NNLO) corrections in the chiral expansion [2–4] lead to perturbative deviations from the LO and involve both computable nonanalytic contributions and analytic terms with some unknown low-energy constants (LEC's), which can be obtained from lattice simulations or experimental measurements.

A combination of some experimental and theoretical inputs from CGL [3, 4], along with the Roy-equation [5, 6], produced a precise result of the  $s$ -wave  $\pi\pi$  scattering lengths. Zhou et al. studied the pole structure of the low-energy  $\pi\pi$  scattering amplitudes using a proper chiral unitarization method in addition to the crossing symmetry and low-energy phase shift data, and estimated

the  $s$ -wave  $\pi\pi$  scattering lengths [7]. K. Sasaki and N. Ishizuka found that the scattering phase can be obtained directly from the  $\pi\pi$  wave function [8]. Guo et al. provided a reliable and solid estimation of all part of the  $\mathcal{O}(p^6)$  calculation [9], and some resonance contributions were added in to the former phenomenological calculations [3, 4], and obtained the slight differences with respect to previous results in Refs. [3, 4]. Using the NLO  $SU(2)$  unitary chiral perturbation theory to examine the  $\pi\pi$  scattering, Albaladejo and Oller obtained a good reproduction of the  $s$ -wave  $\pi\pi$  scattering lengths [10].

In conjunction with the strict  $\chi$ PT constraints in the analysis, the considerably improved accuracy for the  $s$ -wave  $\pi\pi$  scattering lengths has been obtained from the experimental measurement of the semileptonic  $K_{e4}$  decay by E865 [11]. With the independent experimental uncertainties and different theoretical inputs [3, 4, 12], the NA48/2 high-precision analyses of the  $K_{e4}$  and  $K_{3\pi}$  decays [13–16] gave rise to the complementary information on the  $s$ -wave  $\pi\pi$  scattering lengths [15]. All of these theoretical (or phenomenological) predictions and experimental determinations are consistent with each other.

Lattice studies on the  $\pi\pi$  scattering have been conducted in quenched QCD by various groups [17–23]. The full lattice study of the  $s$ -wave  $I = 2$   $\pi\pi$  scattering length was first carried out by CP-PACS [24]. Fully-dynamical computation of the  $I = 2$   $\pi\pi$  scattering was explored by NPLQCD with the domain-wall valence quarks on a fourth-rooted staggered sea quarks [25, 26]. Using the  $N_f = 2$  maximally twisted mass fermion ensembles, Xu et al. employed the lightest pion mass at that time, conducted an explicit check for lattice artifacts [27]. With an anisotropic  $N_f = 2 + 1$  clover fermion discretization, the  $I = 2$   $\pi\pi$  scattering phase shift is calculated by NPLQCD to determine all the threshold parameters [28]. Moreover, efforts were made to first secure the  $d$ -wave  $I = 2$   $\pi\pi$  phase shift in some nice works by HSC [29, 30]. Us-

---

\*Electronic address: fuziwen@scu.edu.cn

ing overlap fermion formulation, Yagi et al. examined the consistency of the lattice data with the NNLO  $\chi$ PT prediction after correcting finite volume effects [31].

Nevertheless, only a couple of lattice studies in the  $I = 0$  channel are reported so far, whose computations are hindered by the so-called “disconnected diagram”. Using the quenched approximation, Kuramashi et al. carried out the pioneering work for isospin-0, however, the vacuum diagram was disregarded assuming that vacuum amplitude remains small for large  $t$  [18]. Additionally, for the rectangular and vacuum diagrams, quark loops are required to make the scattering amplitudes unitary, otherwise, the basic part of the physics is lost due to quenched approximation [17]. Liu conducted the first full QCD calculation for the  $I = 0$  channel including the vacuum graph, however the error of the extracted scattering length is remarkably large due to the usage of big pion masses (small one is 430 MeV) [32]. With the presence of the vacuum diagram, we have attempted to crudely calculate the  $\pi\pi$  scattering for isospin-0, and made a first lattice calculation for  $l_{\pi\pi}^{I=0}(\mu)$ , which is a LEC appearing in the  $\chi$ PT expression of the  $\pi\pi$  scattering length for isospin-0 [33]. Nonetheless, we used the partially quenched QCD to save computational cost, and worked with large quark masses [33]. Moreover, the statistical errors are underestimated since we only considered the primary one [33]. Furthermore, we neglected the obvious oscillating term due to the staggered scheme. We understood that the statistical errors for the ratio of vacuum amplitude grow as  $e^{2m_\pi t}$  [34]. Consequently, using the small quark mass is very important for the  $I = 0$  channel. As presented later, our lattice results will indeed quantitatively confirm this argument, and we acquire the good signals of vacuum diagram for the lattice ensembles with small pion masses.

To overcome the Maiani-Testa theorem [35], people usually calculate the energy levels of two-(many-)particle system enclosed in a torus, and its scattering amplitudes can be recovered [36–49]. In this work, Lüscher’s technique [36–38] is employed to extract the scattering phase shift with the lattice-calculated energy eigenstates.

We here use the MILC gauge configurations [50, 51] with the  $2 + 1$  flavors of the Asqtad-improved staggered dynamical quarks [52] to compute the  $s$ -wave  $\pi\pi$  scattering lengths. The technique of the “moving” wall source without gauge fixing [53] first introduced in Refs. [18, 19] are exploited to calculate all the four diagrams classified in Refs. [17–19], and special effort is paid to the disconnect diagram. Our lightest pion mass is about 240 MeV, which is lighter than those of the former lattice studies on the  $\pi\pi$  scattering and enables us to further explore the chiral limit. Consequently, the signals of vacuum diagram are remarkably improved. Moreover, due to the nature of staggered fermion, our computations are automatically precise to  $\mathcal{O}(a^2)$  [17]. Additionally, we used the continuum three-flavor  $\chi$ PT at NLO to extrapolate our lattice-measured  $\pi\pi$  scattering lengths to the physi-

cal point. As presented later, we find

$$m_\pi a_{\pi\pi}^{I=2} = -0.04430(25)(40); \quad l_{\pi\pi}^{I=2} = 3.27(.77)(1.12),$$

where  $a_{\pi\pi}^{I=2}$  denote the  $s$ -wave  $\pi\pi$  scattering lengths in the  $I = 2$  channel and  $l_{\pi\pi}^{I=2}(\mu)$  is a LEC evaluated at the physical pion decay constant. These results are in well agreement with the experimental measurements and theoretical (or phenomenological) determinations as well as previous lattice calculations. Most of all, we obtain

$$m_\pi a_{\pi\pi}^{I=0} = 0.214(4)(7); \quad l_{\pi\pi}^{I=0} = 43.2(3.5)(5.6),$$

which are in fair accordance with the experimental reports and theoretical (or phenomenological) predictions, and significantly improve our former study in Ref. [33].

The paper is organized as follows. In Sec. II we will review the basic formalism for the calculation of the  $s$ -wave  $\pi\pi$  scattering [37, 38]. The simulation parameters and our concrete lattice calculations are shown in Sec. III. We will give the results of the lattice simulation data in Sec. IV, fitting analyses in Sec. V, and chiral extrapolation along with the comparisons of different results in Sec. VI. Finally, a summary of our conclusions and outlooks are arrived at in Sec. VII. The compact continuum three-flavor  $\chi$ PT forms at NNLO for the  $\pi\pi$  scattering lengths are courteously dedicated in Appendix A.

## II. METHOD

On the basis of the original derivations and notations in Refs. [17–19], we reviewed the indispensable formulas for the lattice QCD evaluation of the  $s$ -wave  $\pi\pi$  scattering lengths in a torus. The formulas and the notations adopted here are actually the same as those in Refs. [33, 54]. But, to make this paper self-supporting, all the essential parts will be reiterated subsequently.

Let us review scattering of two Nambu-Goldstone pions in the Asqtad-improved staggered fermion formalism. For the  $s$ -wave  $\pi\pi$  scattering, only the isospin  $I = 0$  and 2 channels are permitted owing to Bose symmetry. We build these  $\pi\pi$  isospin eigenchannels using the following interpolating operators [18, 19]

$$\begin{aligned} \mathcal{O}_{\pi\pi}^{I=0}(t) &= \frac{1}{\sqrt{3}} \left\{ \pi^-(t)\pi^+(t+1) + \pi^+(t)\pi^-(t+1) - \pi^0(t)\pi^0(t+1) \right\}, \\ \mathcal{O}_{\pi\pi}^{I=2}(t) &= \pi^+(t)\pi^+(t+1), \end{aligned} \quad (1)$$

with the interpolating pion operators denoted by

$$\begin{aligned} \pi^+(t) &= -\sum_{\mathbf{x}} \bar{d}(\mathbf{x}, t)\gamma_5 u(\mathbf{x}, t), \\ \pi^-(t) &= \sum_{\mathbf{x}} \bar{u}(\mathbf{x}, t)\gamma_5 d(\mathbf{x}, t), \\ \pi^0(t) &= \frac{1}{\sqrt{2}} \sum_{\mathbf{x}} [\bar{u}(\mathbf{x}, t)\gamma_5 u(\mathbf{x}, t) - \bar{d}(\mathbf{x}, t)\gamma_5 d(\mathbf{x}, t)], \end{aligned}$$

then we express the  $\pi\pi$  four-point function in the zero momentum state as

$$C_{\pi\pi}(t_1, t_2, t_3, t_4) = \sum_{\mathbf{x}_1} \sum_{\mathbf{x}_2} \sum_{\mathbf{x}_3} \sum_{\mathbf{x}_4} \langle \mathcal{O}_\pi(\mathbf{x}_4, t_4) \mathcal{O}_\pi(\mathbf{x}_3, t_3) \times \mathcal{O}_\pi^\dagger(\mathbf{x}_2, t_2) \mathcal{O}_\pi^\dagger(\mathbf{x}_1, t_1) \rangle,$$

where, to prevent the intricate color Fierz rearrangement of the quark lines [18, 19],<sup>1</sup> we familiarly select  $t_1 = 0$ ,  $t_2 = 1$ ,  $t_3 = t$ , and  $t_4 = t + 1$  [18, 19].

In the isospin limit, only four diagrams contribute to  $\pi\pi$  scattering amplitudes, in Fig. 1, we show these quark-line diagrams, which are identified as direct ( $D$ ), crossed ( $C$ ), rectangular ( $R$ ), and vacuum ( $V$ ) diagrams, respectively [18, 19]. The reliable evaluation of the rectangular diagram is challenging and the rigorous computation of the vacuum diagram is pretty hard [18, 19].

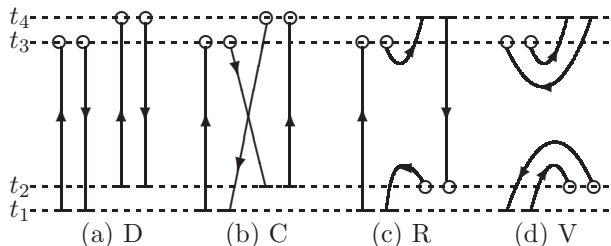


FIG. 1: Quark-line diagrams contributing to  $\pi\pi$  four-point functions. Short bars indicate the wall sources. The wall sinks for local pion operators are represented by open circles.

In our former works [33, 54], we calculated these four diagrams via evaluating  $T$  quark propagators [18, 19]

$$\sum_x D_{n,x} G_t(x) = \sum_{\mathbf{x}} \delta_{n,(\mathbf{x},t)}, \quad 0 \leq t \leq T - 1.$$

The combination of  $G_t(n)$  which we apply for the  $\pi\pi$  four-point functions is schematically illustrated in Fig. 1, and these diagrams can be described by means of  $G$ ,

$$\begin{aligned} C^D(t_1, t_2, t_3, t_4) &= \sum_{\mathbf{x}_3} \sum_{\mathbf{x}_4} \langle \text{Tr}[G_{t_1}^\dagger(\mathbf{x}_3, t_3) G_{t_1}(\mathbf{x}_3, t_3)] \\ &\quad \times \text{Tr}[G_{t_2}^\dagger(\mathbf{x}_4, t_4) G_{t_2}(\mathbf{x}_4, t_4)] \rangle, \\ C^C(t_1, t_2, t_3, t_4) &= \sum_{\mathbf{x}_3} \sum_{\mathbf{x}_4} \langle \text{Tr}[G_{t_1}^\dagger(\mathbf{x}_3, t_3) G_{t_2}(\mathbf{x}_3, t_3) \\ &\quad \times G_{t_2}^\dagger(\mathbf{x}_4, t_4) G_{t_1}(\mathbf{x}_4, t_4)] \rangle, \\ C^R(t_1, t_2, t_3, t_4) &= \sum_{\mathbf{x}_2, \mathbf{x}_3} \langle \text{Tr}[G_{t_1}^\dagger(\mathbf{x}_2, t_2) G_{t_4}(\mathbf{x}_2, t_2) \\ &\quad \times G_{t_4}^\dagger(\mathbf{x}_3, t_3) G_{t_1}(\mathbf{x}_3, t_3)] \rangle, \end{aligned}$$

$$\begin{aligned} C^V(t_1, t_2, t_3, t_4) &= \sum_{\mathbf{x}_2} \sum_{\mathbf{x}_3} \left\{ \langle \text{Tr}[G_{t_1}^\dagger(\mathbf{x}_2, t_2) G_{t_1}(\mathbf{x}_2, t_2)] \right. \\ &\quad \times \text{Tr}[G_{t_4}^\dagger(\mathbf{x}_3, t_3) G_{t_4}(\mathbf{x}_3, t_3)] \rangle \\ &\quad - \langle \text{Tr}[G_{t_1}^\dagger(\mathbf{x}_2, t_2) G_{t_1}(\mathbf{x}_2, t_2)] \\ &\quad \times \left. \langle \text{Tr}[G_{t_4}^\dagger(\mathbf{x}_3, t_3) G_{t_4}(\mathbf{x}_3, t_3)] \right\rangle \}, \quad (2) \end{aligned}$$

where the indicated traces are conducted over color and the  $\gamma^5$  factors are neatly removed using the Hermiticity attributes of the propagator  $G$ , and a vacuum deduction is a natural companion to the vacuum diagram [56].

The rectangular and vacuum diagrams inevitably create the gauge-variant noise [18, 19], which are neatly diminished by executing the gauge field average without gauge fixing as we practiced in Refs. [33, 53, 54, 57–60]. In the isospin limit, the  $\pi\pi$  four-point functions for the  $I = 0$  and 2 channels can be expressed on the strength of four diagrams [17–19],

$$\begin{aligned} C_{\pi\pi}^{I=0}(t) &\equiv \langle \mathcal{O}_{\pi\pi}^{I=0}(t) | \mathcal{O}_{\pi\pi}^{I=0}(0) \rangle = D + \frac{N_f}{2} C - 3N_f R + \frac{3}{2} V, \\ C_{\pi\pi}^{I=2}(t) &\equiv \langle \mathcal{O}_{\pi\pi}^{I=2}(t) | \mathcal{O}_{\pi\pi}^{I=2}(0) \rangle = D - N_f C, \quad (3) \end{aligned}$$

where the staggered-flavor factor  $N_f$  is inserted to rectify for the extra factor  $N_f$  in the valence fermion loops [17]. The four-fold degeneracy of the staggered sea quarks is removed by conducting the quadruple root of the fermion determinant [17, 61]. The fourth-root recipe is assumed to be able to restore the right continuum limit of QCD [61], and our results rest on this hypothesis. See Ref. [62] for more discussions about the fourth-root trick.

It is customary to make use of the effective range expansion for parameterizing the low-momentum behavior of the  $s$ -wave  $\pi\pi$  scattering phase  $\delta_0$ ,

$$k \cot \delta_0(k) = \frac{1}{a} + \frac{1}{2} r k^2 + \mathcal{O}(k^4), \quad (4)$$

where  $a$  is the  $s$ -wave  $\pi\pi$  scattering length,  $r$  is the effective range, and  $k$  is the magnitude of the center-of-mass scattering momentum related to the energy  $E_{\pi\pi}^I$  of the  $\pi\pi$  system with total isospin  $I$  in a torus of size  $L$  by

$$k^2 = \frac{1}{4} (E_{\pi\pi}^I)^2 - m_\pi^2, \quad k = \frac{2\pi}{L} q, \quad (5)$$

here the dimensionless momentum  $q \in \mathbb{R}$ . The  $s$ -wave  $\pi\pi$  scattering length in the continuum limit is denoted by

$$a_0 = \lim_{k \rightarrow 0} \frac{\tan \delta_0(k)}{k},$$

which is purely elastic below inelastic thresholds.<sup>2</sup> We should keep in mind that the truncation of the effective

<sup>1</sup> Fierz contributions force us to overcome the obstacle due to the staggered-flavor symmetry breaking [17]. The same problem is also met for the  $\pi K$  scattering, which is addressed by Lang et al. in Ref. [55]. In principle, they can be disentangled by the way discussed in Ref. [17], but strenuous in practice. Fortunately, it can be trivially handled by the way introduced in Refs. [18, 19], i.e.,  $\pi$  meson operators are separated by a unit time slice.

<sup>2</sup> We are only interested in the elastic region:  $2m_\pi < E_{\pi\pi}^I < 4m_\pi$ , where there is no  $4\pi$  channel, and not up to the opening of the  $K\bar{K}$  channel at around 1 GeV yet [63], where the  $K\bar{K}$  channel contributes remarkably to the isoscalar  $\pi\pi$  interactions [64].

range  $r$  in Eq. (4) is considered as an important source of systematic error, which appears as  $\mathcal{O}(1/L^6)$ . The  $\delta_0(k)$  can be computed by the Lüscher formula [37, 38],

$$k \cot \delta_0(k) = \frac{2\pi}{L} \pi^{-3/2} \mathcal{Z}_{00}(1, q^2), \quad (6)$$

where the dimensionless momentum  $q = kL/(2\pi)$  and the zeta function  $\mathcal{Z}_{00}(1; q^2)$  is formally expressed by

$$\mathcal{Z}_{00}(1; q^2) = \frac{1}{\sqrt{4\pi}} \sum_{\mathbf{n} \in \mathbb{Z}^3} \frac{1}{n^2 - q^2}. \quad (7)$$

We generally compute the zeta function by the method discussed in Ref. [24]. Recently, an equivalent formula is established [65]. It allows us to avoid the subthreshold singularities inherent to Lüscher technique [65].

The energy  $E_{\pi\pi}^I$  can be secured from the  $\pi\pi$  four-point function which manifests as [66]

$$C_{\pi\pi}^I(t) = Z_{\pi\pi} \cosh \left[ E_{\pi\pi}^I \left( t - \frac{1}{2}T \right) \right] + (-1)^t Z_{\pi\pi}^I \cosh \left[ E_{\pi\pi}^{II} \left( t - \frac{1}{2}T \right) \right] + \dots \quad (8)$$

for a large  $t$  to reduce the excited states, the terms alternating in sign is a representative feature of a staggered scheme [66], and the ellipsis indicates the contributions from the excited states which are suppressed exponentially. In practice, the pollution due to the “wraparound” effects [21, 27, 67] should be taken into account.

It should be worth to stress that, even if we project onto the Goldstone pions at source and sink timeslices, pions with all 16 staggered-flavors still emerge at the intermediate times [17]. However, in large  $t$ , the contributions of non-Goldstone pions in the intermediate states is exponentially reduced due to their heavier masses in contrast with those of the Goldstone pions [17–19].

In practice, for the sake of a more intuitive presentation of our results, we compute the ratios <sup>3</sup>

$$R^X(t) = \frac{C_{\pi\pi}^X(0, 1, t, t+1)}{C_{\pi}(0, t)C_{\pi}(1, t+1)}, \quad X = D, C, R, \text{ and } V, \quad (9)$$

where  $C_{\pi}(0, t)$  and  $C_{\pi}(1, t+1)$  are pion correlators with zero momentum. With the consideration of Eq. (3), we can depict the  $\pi\pi$  scattering amplitudes which project out the  $I = 0$  and 2 isospin eigenstates as

$$\begin{aligned} R_{I=0}(t) &= R^D(t) + \frac{1}{2}N_f R^C(t) - 3N_f R^R(t) + \frac{3}{2}R^V(t), \\ R_{I=2}(t) &= R^D(t) - N_f R^C(t). \end{aligned} \quad (10)$$

<sup>3</sup> In principle, when  $t \ll T/2$ , even if placing the periodic boundary condition in the temporal direction, the energy shift of the  $\pi\pi$  system can be still roughly evaluated from these ratios. In this work we do not use these ratios to quantitatively calculate any physical quantities, nonetheless, these ratios will indeed help us comprehend qualitatively or intuitively some physical quantities.

In this work, we will employ two approaches to calculate the pion mass  $m_{\pi}$ . The first method is to use both the point-source and point-sink operator. Nevertheless, the point operator has big overlap with excited states [68], and in practice it is customary to use the wall-source operator which efficiently reduces these overlaps, along with a point-sink [68]. In addition we need both propagators to calculate pion decay constant [50, 51].

### III. LATTICE CALCULATION

We used the MILC gauge configurations [50, 51] with the 2 + 1 flavors of asqtad-improved staggered sea quarks [52] and a Symanzik-improved gluon action [69]. See detailed simulation parameters in Ref. [70]. It is worth mentioning that the MILC gauge configurations are generated using the staggered formulation of lattice fermions [71] with the fourth-root of fermion determinant which are hypercubic-smear (HYP-smear) [72]. As shown in Ref. [73], the chiral symmetry are significantly enhanced via the HYP-smear gauge link.

The lattice simulation parameters of the MILC gauge configurations used here are epitomized in Table I. The simulated bare masses of light and strange sea quarks are denoted by  $am_l$  and  $am_s$ , respectively. The masses of the  $u$  and  $d$  quarks are degenerate, which are small enough, such that the physical up- and down-quark masses can be attained by the chiral extrapolation. The lattice spacing  $a$  for first three lattice ensembles is about 0.12 fm, and that of last three lattice ensembles is around 0.15 fm. By MILC convention, the lattice ensembles are referred to as “coarse” for  $a \approx 0.12$  fm, and “medium-coarse” for  $a \approx 0.15$  fm. For easy notation, it is convenient to use  $(am_l, am_s)$  to mark lattice ensembles, e.g., “the (0.01, 0.05) ensemble”. The tadpole factors  $u_0$  [74] are utilized to enhance the gauge configuration action [50, 51].

To compute the  $\pi\pi$  four-point functions  $C_{\pi\pi}(t)$ , the standard conjugate gradient technique <sup>4</sup> is used to acquire the required matrix element of inverse fermion matrix. The periodic boundary condition is applied to the three spatial directions and temporal direction. We compute  $C_{\pi\pi}(t)$  on all the possible time slices, and collect them at the end of the measurement, namely,

$$C_{\pi\pi}(t) = \frac{1}{T} \sum_{t_s=0}^{T-1} \langle (\pi\pi)(t+t_s) (\pi\pi)^\dagger(t_s) \rangle.$$

After averaging the correlators over all the  $T$  possible values of common time shift  $t_s$ , as illustrated later, we found that the statistics are indeed significantly improved.

<sup>4</sup> The conjugate gradient residual used in this work is  $1.0 \times 10^{-5}$ , which is smaller than that used in generating gauge configurations [50, 51]. Moreover, to avoid the potential roundoff errors as much as possible, all the numerical calculations are calculated in double precision.

TABLE I: The parameters of MILC gauge configurations used in the present work. The lattice dimensions are expressed in lattice units in the second block with spatial ( $L$ ) and temporal ( $T$ ) size. The gauge coupling  $\beta = 10/g^2$  is shown in Column three. The fourth and fifth blocks give the bare masses of the light and strange quark masses in terms of  $am_l$  and  $am_s$ , respectively. Tadpole-improvement factor  $u_0$  is listed in Column six. The ratio  $r_1/a$  is provided in Column seven (see Ref. [75] for the MILC definition of  $r_1$ ). The inverse lattice spacing  $a^{-1}$  is recapitulated in Column eight (for the (0.00484, 0.0484) ensemble, we obtain the value of  $r_1/a$  from Ref. [70], then calculate  $a^{-1}$ ). In the last column the number of gauge configurations is given.

Ensemble	$L \times T$	$\beta$	$am_l$	$am_s$	$u_0$	$r_1/a$	$a^{-1}\text{GeV}$	$N_{cf}$
$a \approx 0.12 \text{ fm}$								
2464f21b676m005m050	$24^3 \times 64$	6.76	0.005	0.050	0.8678	2.647(3)	$1.679^{+43}_{-16}$	156
2064f21b676m007m050	$20^3 \times 64$	6.76	0.007	0.050	0.8678	2.635(3)	$1.672^{+43}_{-16}$	200
2064f21b676m010m050	$20^3 \times 64$	6.76	0.010	0.050	0.8677	2.619(3)	$1.663^{+43}_{-16}$	200
$a \approx 0.15 \text{ fm}$								
2048f21b6566m00484m0484	$20^3 \times 48$	6.566	0.00484	0.0484	0.8602	2.162(5)	$1.373^{+34}_{-14}$	560
1648f21b6572m0097m0484	$16^3 \times 48$	6.572	0.0097	0.0484	0.8604	2.140(4)	$1.358^{+35}_{-13}$	250
1648f21b6586m0194m0484	$16^3 \times 48$	6.586	0.0194	0.0484	0.8609	2.129(3)	$1.352^{+35}_{-13}$	200

For each time slice, three fermion matrix inversions are needed corresponding to the 3 color choices for the pion source, and each inversion takes about 1000 iterations (about 2000 for the (0.00484, 0.0484) and (0.005, 0.05) ensembles) during the conjugate gradient calculation. Thus, totally we carry out  $3T$  inversions on a single gauge configuration. As shown later, this rather big number of the inversions offers the substantial statistics needed to get the  $\pi\pi$  scattering amplitudes with high accuracy.

In practice, we calculate the pion correlators,

$$C_\pi^{\text{PP}}(t) = \frac{1}{T} \sum_{t_s=0}^{T-1} \langle 0 | \pi^\dagger(t+t_s) \pi(t_s) | 0 \rangle,$$

$$C_\pi^{\text{WP}}(t) = \frac{1}{T} \sum_{t_s=0}^{T-1} \langle 0 | \pi^\dagger(t+t_s) W_\pi(t_s) | 0 \rangle, \quad (11)$$

where  $\pi$  is the pion point-source operator and  $W_\pi$  is the pion wall-source operator [50, 51]. To simplify the notation in this section, the summation over the lattice space point in sink is not written out. In this work, we will adopt the shorthand notation: “PP” for the point-source point-sink propagators, and “WP” for the wall-source point-sink propagators [51]. We should stress that the summations are also taken over all the time slice for the pion propagators, and we found that the statistics are indeed significantly improved. This is very important to obtain pion mass with high accuracy.

Overlooking the excited state contributions, the pion mass  $m_\pi$  can be secured at large  $t$  with a single exponential fit ansatz [61, 70, 76]

$$C_\pi^{\text{PP}}(t) = A_\pi^{\text{PP}} \left[ e^{-m_\pi t} + e^{-m_\pi(T-t)} \right], \quad (12)$$

$$C_\pi^{\text{WP}}(t) = A_\pi^{\text{WP}} \left[ e^{-m_\pi t} + e^{-m_\pi(T-t)} \right], \quad (13)$$

where  $T$  is the temporal extent of the lattice,  $A_\pi^{\text{PP}}$  and  $A_\pi^{\text{WP}}$  are overlapping amplitudes. We will use these values to estimate the wrap-around contributions [21, 27, 67] and calculate the pion decay constant [68] as well.

We should remark at this point that, in the calculation of the  $\pi\pi$  four-point functions for the  $I = 0$  channel, we try our best effort to compute the vacuum diagram, since the other three diagrams can be relatively easily calculated. We found that the vacuum diagram plays a critical role in this correlator.<sup>5</sup>

## IV. LATTICE SIMULATION RESULTS

### A. Pion mass and pion decay constant

In practice, the  $\pi$  propagators were fit by varying minimum fitting distances  $D_{\min}$ , and with maximum distance  $D_{\max}$  either at  $T/2$  or where the fractional statistical errors surpassed about 20% for two sequential time slices [50, 51, 61].<sup>6</sup> In this work, pion masses were secured from the “effective mass” plots for each of the MILC lattice ensembles, and they were strenuously opted by looking for a combination of a “plateau” in the mass as a function of  $D_{\min}$ , good fit quality (i.e.,  $\chi^2/\text{dof} \leq 1$ ), and  $D_{\min}$  large enough to reduce the excited states [25–27]. The WP propagators were fit to Eq. (13) using a minimum time distance of  $14a$  for the “medium-coarse” lattices and  $20a$  for the “coarse” lattices, and the full covariance matrix is used to compute statistical errors. At these large distances, the pollution from excited states is at most comparable to the statistical errors [68]. For example, Fig. 2 exhibits the results for pion masses and amplitudes as a function of  $D_{\min}$  for the (0.007, 0.05)

<sup>5</sup> In our previous work [77], we presented the detailed procedure to calculate the disconnected diagram for the  $f_0(600)$  meson. It helps us a lot to implement the evaluation of the vacuum diagram here, especially for how to conduct a vacuum subtraction.

<sup>6</sup> Since the lattice data points at the largest distances contain relatively little information, the exact selection of large distance cutoff  $D_{\max}$  is not very critical [50, 51, 61].

ensemble. Since the major objective of this work is to present the work for isospin-0, as explained later, for the  $\pi\pi$  scattering in the  $I = 0$  channel at this work, the systematic error of the energy of the  $\pi\pi$  system is pretty large, we can temporarily neglect the systematic effect for pion mass due to excited states. All of these fitted values of pion masses are listed in Table II.

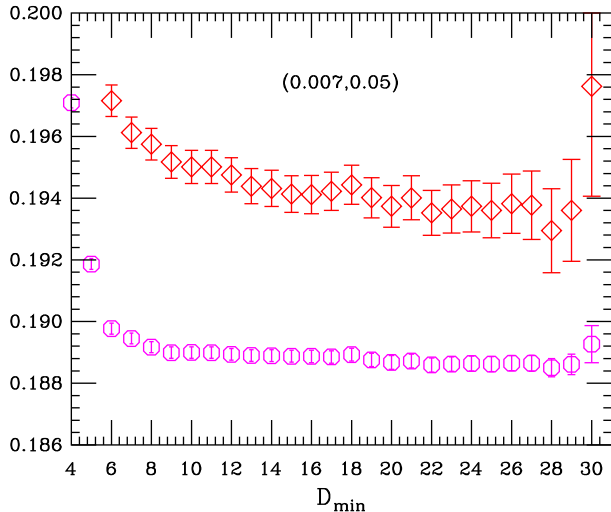


FIG. 2: (color online). Pion masses (magenta octagons) and WP amplitudes  $A_{\pi}^{\text{WP}}$  (red diamonds) as a function of the minimum time distance in the fit for the (0.007, 0.05) ensemble. The amplitudes have been divided by 2060.

In our previous work [33], we used the method described in Ref. [68] to extract the pion decay constant for the (0.0097, 0.0484) ensemble [33]. In the light of same procedures, we calculated the pion decay constants for other “medium coarse” ensembles. All of these fitted values of pion decay constants are listed in Table II.

As a consistency check, the PP correlators were reliably measured in this work. Use these correlators, we can secure pion masses via Eq. (12) which are listed in last block in Table II, and these pion masses are found to be consistent with its counterparts extracted with WP propagators, which are summarized in Table II.

Our fitted values of pion masses and pion decay constants listed in Table II, are in rather good agreement with the same quantities which are computed on the same lattice ensembles by MILC collaboration in Refs. [70, 76]. For the “coarse” ensembles, the MILC’s determinations on pion decay constants are directly quoted [70, 76], which are also summarized in Table II.

## B. Diagrams $D, C, R$ , and $V$

As practiced in our former work [33], the  $\pi\pi$  four-point functions are robustly calculated on six MILC lattice ensembles listed in Table I using the technique of the moving wall source without gauge fixing [18, 19, 53]. In Fig. 3, the individual ratios, which are denoted in Eq. (9),  $R^X$

( $X = D, C, R$  and  $V$ ) are illustrated as the functions of  $t$  for each lattice ensemble.

The ratio values of the direct amplitude  $R^D$  are quite close to oneness, indicating a pretty weak interaction in this channel. The crossed amplitude, in another aspect, increases linearly up to  $t \sim 18$  for the “medium coarse” ensemble and  $t \sim 24$  for the “coarse” ensemble, implying a repulsive interaction between two pions in the  $I = 2$  channel. In contrast, after a beginning increase up until  $t \sim 4$ , the rectangular amplitude demonstrates a roughly linear decrease up until  $t \sim 18$  for the “medium coarse” ensemble and  $t \sim 24$  for the “coarse” ensemble, suggesting an attractive force among two pions for the  $I = 0$  channel. Additionally, the magnitude of the slope is similar to that of the crossed amplitude but with opposite sign. Furthermore, we observe that the crossed and rectangular amplitudes have the same values at  $t = 0$  and close ones for small  $t$ . These characteristics are in good keeping with the theoretical predictions [17].

It is extremely noisy in the amplitude of the vacuum diagram ( $V$ ) for the (0.0194, 0.0484) ensemble, while we can see a good signal up to  $t = 10$ , and loss of signals after that. These characteristics are in well accordance with the Okubo-Zweig-Iizuka (OZI) rule and  $\chi$ PT in leading order, which expect the disappearing of the vacuum amplitude [17–19]. For the lattice ensembles with the pion mass changing smaller, the signals of the vacuum diagram are becoming more and more tolerating. For the (0.00484, 0.0484) ensemble, the signals of the vacuum diagram is already tolerating. This qualitatively confirmed the analytical arguments in Ref. [34] which indicates that the error of the vacuum amplitude grows exponentially as  $e^{2m_{\pi}t}$ . The numerical calculation of the amplitude for the vacuum diagram stands as our principal and distinctive accomplishment of this paper.

The systematically oscillating behavior of the rectangular amplitude in large  $t$  is evidently observed, which is a typical feature of the staggered formulation of lattice fermions and corresponds to the contributions from the intermediate states with opposite parity [66], and for the lattice ensemble with large pion mass, this oscillating feature become more obvious. In contrast, for that with small pion mass, this feature is not appreciable, and even not perceptible for the MILC (0.00484, 0.0484) ensemble. The physical meaning of this fascinatingly oscillating behavior is easily understood [66]. Nevertheless, its quantitative mass dependence is not clear to us, which are highly needed to be further investigated.

## C. The errors of $R^V(t)$ and $R^R(t)$

According to the analytical arguments in Ref. [34], the error of the ratio for the vacuum amplitude increases exponentially as  $e^{2m_{\pi}t}$ . Therefore, it is pretty difficult to secure the correct signal for large  $t$  [34]. Likewise, the ratio for the rectangular diagram has errors, which grow exponentially as  $e^{m_{\pi}t}$  for large  $t$  [34]. Our lattice data

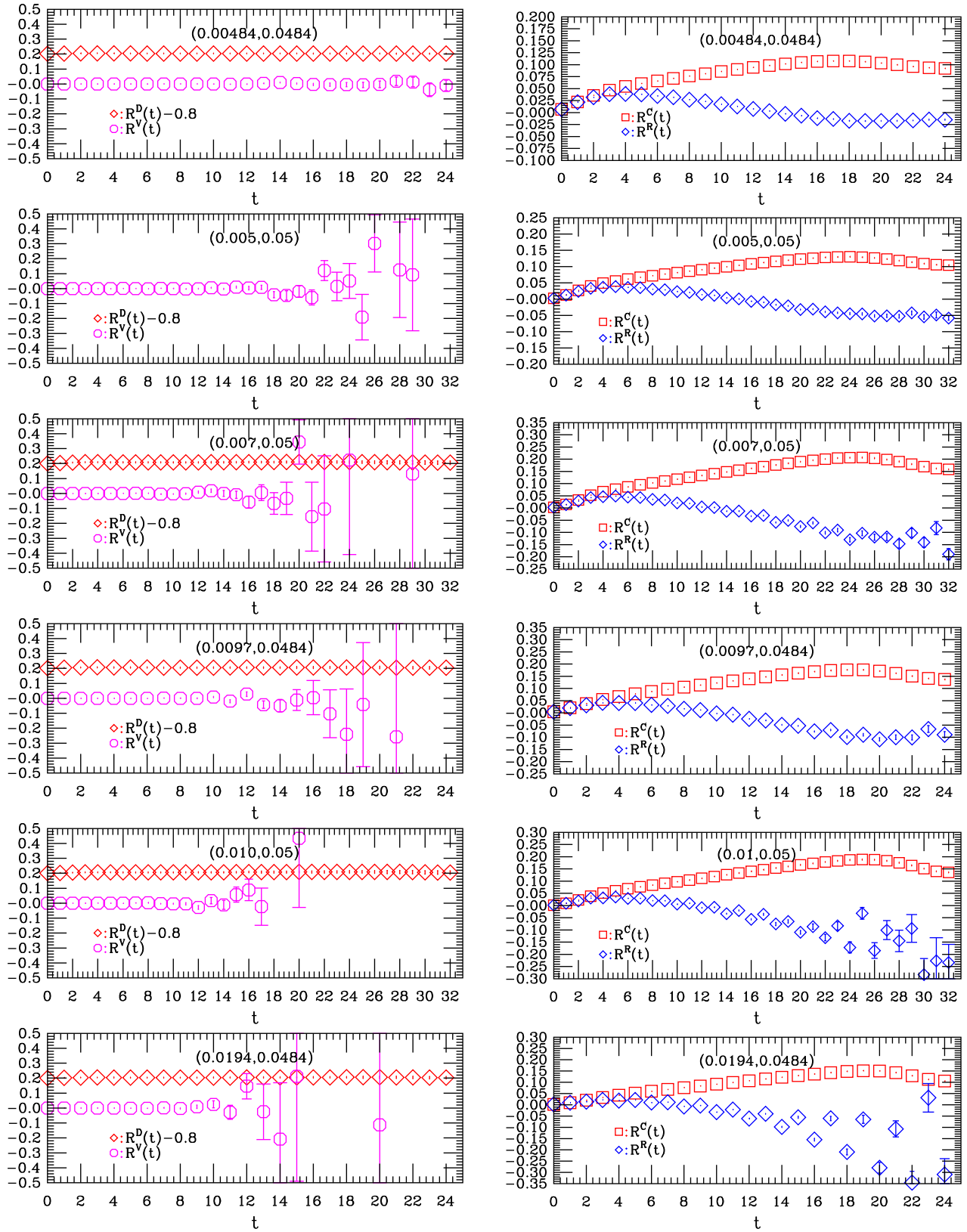


FIG. 3: (color online). Individual amplitude ratios  $R^X(t)$  of the  $\pi\pi$  four-point functions computed via the moving wall source without gauge fixing as the functions of  $t$  for six MILC lattice ensembles. Direct diagram (red diamonds) displaced by 0.8, vacuum diagram (magenta octagons), crossed diagram (red squares) and rectangular diagram (blue diamonds).

TABLE II: Summaries of the pion masses and pion decay constants. The third block shows the pion masses in lattice units and the fifth block give the overlapping amplitude using WP propagators. The product of  $m_\pi L$  is presented in Column four. The pion decay constants in lattice units are provided in sixth block, where the star on the superscript indicate the MILC's determination. Column two shows the values of pion mass in MeV, where the errors are estimated from both the error on lattice spacing  $a$  and statistical errors in Column three. The seven block shows the dimensionless ratio  $m_\pi/f_\pi$ , where the errors are estimated from the  $am_\pi$  and  $af_\pi$ . The last block shows the pion masses which are measured by the point-wall point-sink propagators, and only used as a consistency check.

Ensemble	$m_\pi(\text{MeV})$	$am_\pi^{\text{WP}}$	$m_\pi^{\text{WP}}L$	$A_\pi^{\text{WP}}$	$af_\pi$	$m_\pi/f_\pi$	$am_\pi^{\text{PP}}$
(0.00484, 0.0484)	240(4)	0.17503(09)	3.5006(18)	$1000.18 \pm 1.580$	0.11767(45)	1.4874(57)	0.17504(09)
(0.005, 0.05)	268(5)	0.15970(15)	3.8345(48)	$770.534 \pm 2.577$	0.09054(33)*	1.7639(66)	0.15992(16)
(0.007, 0.05)	315(6)	0.18868(22)	3.7736(44)	$399.094 \pm 1.393$	0.09364(20)*	2.0149(49)	0.18871(24)
(0.0097, 0.0484)	334(6)	0.24566(18)	3.9306(29)	$395.107 \pm 1.151$	0.12136(29)	2.0242(51)	0.24587(21)
(0.01, 0.05)	373(7)	0.22455(27)	4.4910(54)	$365.595 \pm 2.039$	0.09805(14)*	2.2902(42)	0.22447(17)
(0.0194, 0.0484)	463(8)	0.34279(19)	5.4846(30)	$315.695 \pm 0.865$	0.13055(48)	2.6258(98)	0.34279(23)

indeed demonstrates such dependence with the expected slopes.

The magnitudes of these errors are quantitatively in line with these analytical predictions as demonstrated in Fig. 4. Fitting the errors  $\delta R^V(t)$  and  $\delta R^R(t)$  by a single exponential fit ansatz  $\delta R^V(t) \sim e^{\mu_V t}$  and  $\delta R^R(t) \sim e^{\mu_R t}$ , respectively, for six lattice ensembles, we extract the fitted values of  $\mu_V$  and  $\mu_R$ , which are summarized in Table III, together with their fitting ranges.

TABLE III: Summaries of the fitted values for  $\mu_V$  and  $\mu_R$  in lattice units. The second and third blocks show the fitted values of  $\mu_V$ , and  $\mu_R$ , respectively, and Column four gives the time range for the chosen fit.

Ensemble	$a\mu_V$	$a\mu_R$	Range
(0.00484, 0.0484)	0.3392	0.1621	10 – 18
(0.0097, 0.0484)	0.4956	0.2457	8 – 16
(0.0194, 0.0484)	0.6927	0.3487	8 – 16
(0.005, 0.05)	0.3178	0.1513	10 – 20
(0.007, 0.05)	0.3701	0.1895	10 – 20
(0.01, 0.05)	0.4463	0.2237	10 – 20

From Table III, we note that the fitted values of  $\mu_R$  can be compared with the pion masses  $m_\pi$  listed in Table II, and half of the fitted values of  $\mu_V$  can also be reasonably compared with these pion masses. We here have numerically confirmed the Lepage's analytical arguments [34] about the  $\pi\pi$  scattering. This testifies the practical applicability of the moving wall source without gauge fixing from another point of view. Thus, we can reasonably assume that the vacuum amplitude remains small for large  $t$ . In principle, we can overlook the vacuum amplitude in the rest of the analysis. However, we will explicitly include it for the sake of completeness of the lattice QCD calculation.

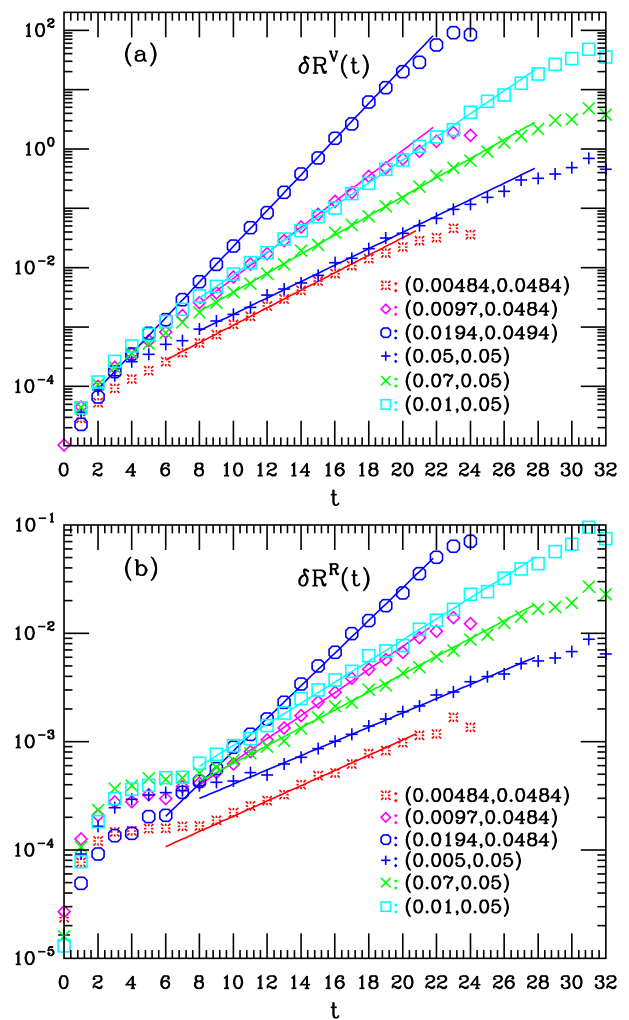


FIG. 4: (color online). The errors of the amplitude ratios  $R^X(t)$  ( $X = V, R$ ) as the functions of  $t$  for each of the MILC lattice ensembles. Solid lines are single exponential fits, and the fitting ranges are listed in Table III. (a) The errors of the amplitude ratios  $R^V(t)$ ; (b) Those of  $R^R(t)$



### D. $R_I$ projected onto the $I = 0$ and 2 channels

The ratios  $R_I(t)$  projected onto the isospin  $I = 0$  and 2 eigenchannels for the MILC (0.00484, 0.0484) and (0.005, 0.05) ensembles, are demonstrated in Fig. 5. A decrease of the ratio  $R_{I=2}(t)$  indicates a repulsive interaction among two pions for the  $I = 2$  channel, on the other hand, an increase of the ratio  $R_{I=0}(t)$  suggests an attractive interaction for the  $I = 0$  channel. In the  $I = 0$  channel, a dip at  $t = 3$  for the (0.00484, 0.0484) and  $t = 5$  for the (0.005, 0.05) can be clearly observed, and its physical origin is not clear to us as well [18, 19].

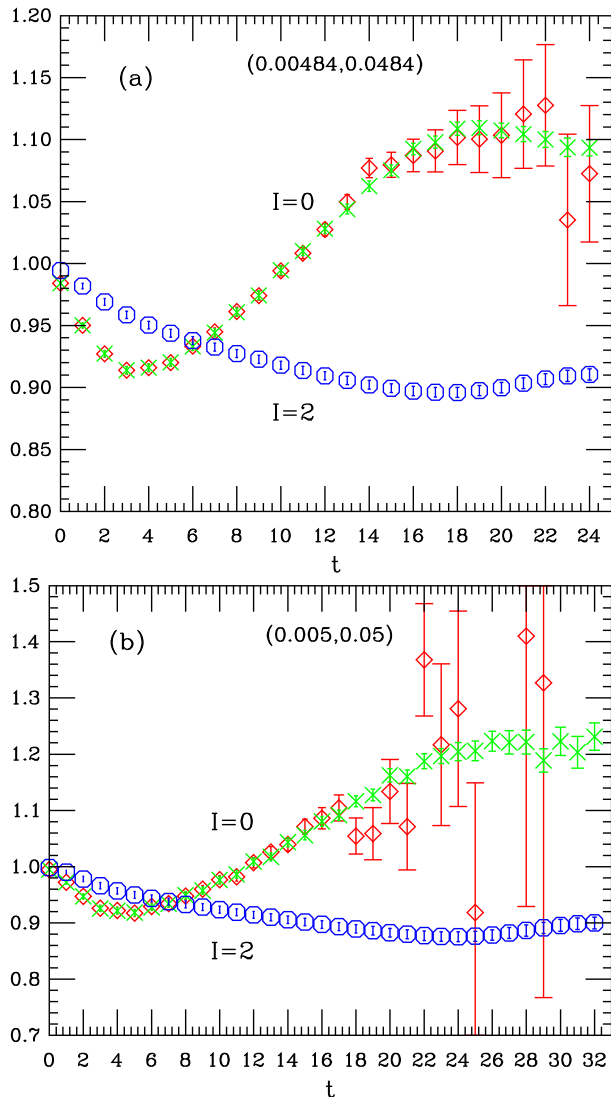


FIG. 5: (color online).  $R_I(t)$  ( $I = 0$  and 2) for the  $\pi\pi$  four-point function at zero momenta calculated by the moving wall source without gauge fixing as the functions of  $t$  for the MILC lattice (a) (0.00484, 0.0484) ensemble; and (b) (0.005, 0.05) ensemble. The cross yellow points indicate the ratio  $R_I(t)$  in the  $I = 0$  channel where the vacuum diagram is turned off.

Due to the rather small quark mass of two lattice ensembles, the systematically oscillating behavior for the

$I = 0$  channel in large  $t$  is not clearly observed, which is a typical characteristic of the Kogut-Susskind formulation of lattice fermions [66]. Additionally, this oscillating feature is hardly noticed for the  $I = 2$  channel.

In order to present the contribution from the vacuum term more intuitively, we employ the yellow cross points to indicate the ratio  $R_I(t)$  for the  $\pi\pi$  four-point function in the  $I = 0$  channel without the presence of the disconnected diagram. From Fig. 5, we can clearly notice that the contribution from the disconnected diagram is only obvious when  $t \geq 20$  for the (0.00484, 0.0484) ensemble, and  $t \geq 16$  for the (0.005, 0.05) ensemble.

### E. Lattice artifact

From Fig. 3, we observe that there exists a pollution from the “wraparound” effects [21, 27, 67] approximately starting as early as at  $t = 12 \sim 18$  for the MILC “medium-coarse” ensembles and  $t = 22 \sim 25$  for the “coarse” ensembles. As discussed in Refs. [21, 27, 31, 67], one of two pions can propagate  $T - t$  time steps backwards due to the periodic boundary condition in the temporal direction. This operates as a constant contribution and deforms the  $\pi\pi$  four-point functions in large  $t$  (especially around  $T/2$ ), according to the discussions in Refs. [21, 27, 31, 67], it is roughly suppressed by

$$\exp(-m_\pi T) / \exp(-2m_\pi t)$$

as compared with forward propagation of the  $\pi\pi$  state. We can opt the fitting ranges satisfying  $t_{\max} \ll T/2$  to reduce this effect [21]. However, according to the arguments in Refs. [21, 27, 31, 67], if pion mass is small enough (e.g. the (0.00484, 0.0484) ensemble), the wrap-around pollution can not be suppressed even for  $t \ll T/2$ , we should include this term for the successful fit,<sup>7</sup>

$$C_{\pi\pi}^I(t) = C + A_{\pi\pi} \cosh[E_{\pi\pi}^I(t - \frac{1}{2}T)] + (-1)^t A'_{\pi\pi} \cosh[E'_{\pi\pi}(t - \frac{1}{2}T)] + \dots \quad (14)$$

where  $C$  is a constant corresponding to the wrap-around term. This can be easily understood by evaluating the contribution of two fake diagrams in Fig. 2 of Ref. [31], and the  $C$  can be expressed as

$$C = 2A_\pi^2 e^{-m_\pi T}. \quad (15)$$

For easy notation the superscript WP in  $A_\pi$  is omitted in the rest of analyses.

In this work, we accurately extract the overlapping amplitudes  $A_\pi$  and pion masses  $m_\pi$  corresponding to pion

<sup>7</sup> It turned out that a five-parameter cosh-fit of  $C$ ,  $A_{\pi\pi}$ ,  $E_{\pi\pi}^I$ ,  $A'_{\pi\pi}$ , and  $E'_{\pi\pi}$  yields a satisfactory result with an pretty acceptable  $\chi^2$ . Moreover, the excited states will be taken into account as one of the important sources of systematical error in this work.

correlators [78] which are listed in Table II, and these values are sufficiently precise to estimate the wraparound terms with Eq. (15), which are listed in Table IV.

TABLE IV: Summaries of the calculated wraparound contributions from overlapping amplitude  $A_\pi$  and pion mass  $am_\pi$ . The second block shows the wraparound contributions calculated from Eq. (15), where its errors are roughly estimated from the statistical errors of  $A_\pi$  and  $m_\pi$ .

Ensemble	$C$
(0.00484, 0.0484)	451.36(2.63)
(0.005, 0.05)	43.23(51)
(0.007, 0.05)	1.815(29)
(0.0097, 0.0484)	2.362(25)
(0.01, 0.05)	0.1533(31)
(0.0194, 0.0484)	0.01424(15)

We note that Ref. [30] has recently taken the similar definition as

$$C = 2A_{\pi\pi}e^{-m_\pi T}, \quad (16)$$

where  $A_{\pi\pi}$  is defined in Eq. (14). Additionally, there exists the similar general form which contains the two-particle as well as one-particle eigenvalues, and gives a not rigorous proof in Ref. [79]. Furthermore, when studying  $K \rightarrow \pi\pi$  decay amplitudes, there is an analogous fitting functional form in Ref. [56].

In order to comprehend this wraparound effects at a quantitative level, we denote a quantity

$$R_{WC}(t) = \frac{C}{C_{\pi\pi}^{I=2}(t)}, \quad (17)$$

which is the ratio of the wraparound pollution to the  $\pi\pi$  four-point function in the  $I = 2$  channel. In fact, we exploited the data of the wraparound contribution  $C$  listed in Table IV and  $C_{\pi\pi}^{I=2}(t)$  calculated from Eq. (3) to approximately evaluate these ratios. The ratios for six MILC lattice ensembles are illustrated in Fig. 6. All of these ratios make a significant contribution and are approximately close to 1/2 as  $t$  approaches to  $T/2$  as expected from the arguments in Refs. [21, 27, 31, 67]. We can note that as the pion mass of the lattice ensemble becomes smaller, the wraparound contribution  $C$  is clearly observed even at small  $t$ . For example, we can keenly notice the wrap-around term even as early as at  $t = 10 \sim 12$  satisfying  $t \ll T/2$  for the (0.00484, 0.0484) ensemble. It is, therefore, absolutely necessary for us to explicitly consider the wrap-around term, especially for lattice ensembles with small pion masses when we extract the energy  $E$  of the  $\pi\pi$  system [31].

To get rid of this pollution, Xu et al. [27] employed a derivative method and denoted a modified ratio [67]. By ignoring terms suppressed relative to the leading contribution, the energy shift  $\delta E$  can be obtained from the asymptotic form of the modified ratio. To identify the

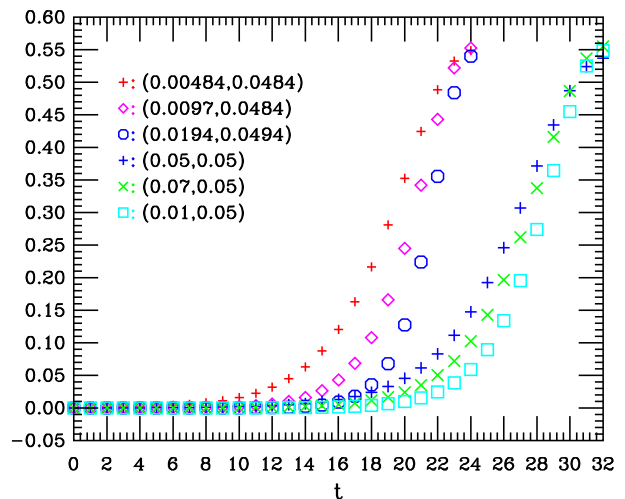


FIG. 6: (color online). The ratios of the wraparound terms to the corresponding  $\pi\pi$  four-point functions for six MILC lattice ensembles calculated by Eq. (17). All of these ratios make a significant contribution and are approximately close to 1/2 as  $t$  approaches to  $T/2$  as expected from the arguments in Refs. [21, 27, 31, 67].

time-separations where the ground state dominates, Yagi et al. used their self-defined ratios [31]. Moreover, Dudek et al. [30] recently eliminated this unwanted pollution term by the shifted correlator.

In principle, we can use one of the three above-mentioned methods to process our  $\pi\pi$  scattering data for isospin-2. However, for those of the  $I = 0$  channel, there is a further complication introduced by staggered fermions, the oscillating term is appreciable, we must consider the oscillating term and modify the corresponding functional forms, as a consequence, it is not convenient to use these methods. Additionally, for the pion-kaon ( $\pi K$ ) scattering [53, 78], and the  $\pi\pi$  correlators “in flight” [30], the wrap-around term is not a constant, and these methods are not suitable.

Nagata et al. solved this problem by subtracting the wrap-around term numerically from the obtained quantities [78], since the lattice-measured data are sufficiently precise to allow such subtraction. Dudek et al. eliminated this term by means of the shifted correlator for the  $\pi\pi$  scattering at rest and weighted-shifted correlator for that “in flight” [30]. We already exhibited that the overlapping amplitude  $A_\pi$  and pion mass  $m_\pi$  can be calculated with high accuracy, so, it is natural to borrow these methods to our case [30, 78]. As a consistency check, we numerically compared these results calculated from the above-mentioned methods for lattice data in the  $I = 2$  channel, and found that they are well consistent with each other within errors. Therefore, in this work we only present the results from the last method, namely, using equation (14) to extract the energy  $E$  of the  $\pi\pi$  system in a conceptually clean way.

## V. FITTING ANALYSES

As already explained in previous sections, we will use Eq. (14) to get the energies  $aE$  of the  $\pi\pi$  system, which are inserted into the Lüscher formula (6) to obtain the corresponding  $s$ -wave  $\pi\pi$  scattering lengths. Hence, appropriately extracting the energies is a central step to our ultimate results. A persuasive way to process our lattice data is the resort to the “effective energy” plot, which is a variant of the effective mass plot, and very similar to the “effective scattering length” plot [25, 26].

### A. $I = 2$ channel

In practice,  $\pi\pi$  four-point functions were fit by varying the minimum fitting distances  $D_{\min}$ , and with the maximum distance  $D_{\max}$  either at  $T/2$  or where the fractional statistical errors surpassed about 20% for two sequential time slices [50, 51, 61]. Additionally, the fitting parameter  $C$  was constrained by priors to conform the lattice-calculated wraparound contribution  $C$  listed in Tables IV [80]. For each ensemble, the “effective energy” plots as a function of  $D_{\min}$  are illustrated in Fig. 7. The central value and statistical error at each time slice were evaluated by the Levenberg-Marquardt algorithm [81]. To make these fits more robust, we double-check them with SNOBFIT, which is a soft constrained noisy optimization [82]. From Fig. 7, we also observed that the effective energies have larger statistical errors near  $t \sim T/2$  because of the wrap-around effect as it is discussed in detail in Ref. [31].

We should remark that the physical model in Eq. (14) just include the ground state [25–27]. In fact, we can fit with the inclusion of the first excited state, and the difference between these procedures, as well as the difference arising from the arbitrary choice of  $D_{\max}$ , is incorporated in the systematic error for  $aE$  at each time slice.

In this work, the energies  $aE$  of the  $\pi\pi$  system in the  $I = 2$  channel were secured from the “effective energy” plots for each of the MILC lattice ensembles, and they were strenuously opted by looking for a combination of the “plateau” in the energy as the function of  $D_{\min}$ , good fit quality [25–27], and  $D_{\min}$  large enough to suppress the excited states. We found that the effective energy of the  $\pi\pi$  system for the  $I = 2$  channel have relatively small errors within a broad minimum time distance region.

For the same fitting range, analogously we secured the wraparound term  $C$  from the corresponding “effective wraparound constant” plots in Fig. 8. It is worth mentioning that the fitted wraparound pollution  $C$  are in fair agreement with the calculated wraparound pollution  $C$  within errors. Nonetheless, it is interesting to note that there exist about 1% differences, and the physical indication is not clear to us, which are highly needed to be further investigated in the future work.

The fitted values of the energies  $aE$  of the  $\pi\pi$  system with isospin-2, fitting range and fit quality ( $\chi^2/\text{dof}$ ) are

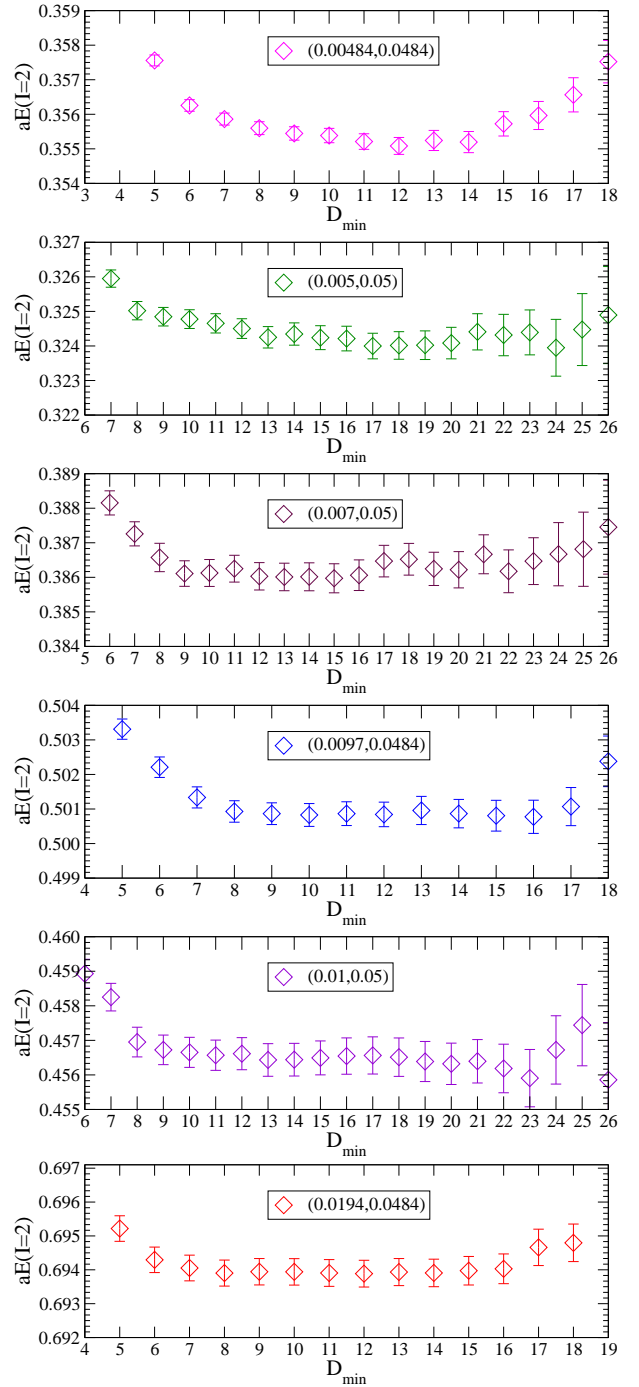


FIG. 7: (color online). The “effective energy” plots as the functions of  $D_{\min}$  for the  $\pi\pi$  scattering in the  $I = 2$  channel in lattice units. The “effective energy” plots have small errors within a broad minimum fitting distance region. The estimates of the systematic uncertainty due to fitting are not displayed in this figure.

tabulated in Table V, together with the fitted values of the wraparound contribution  $C$ . We note that the fitted values of  $C$  is a statistically significant constant term de facto for the lattice ensembles with small pion masses.

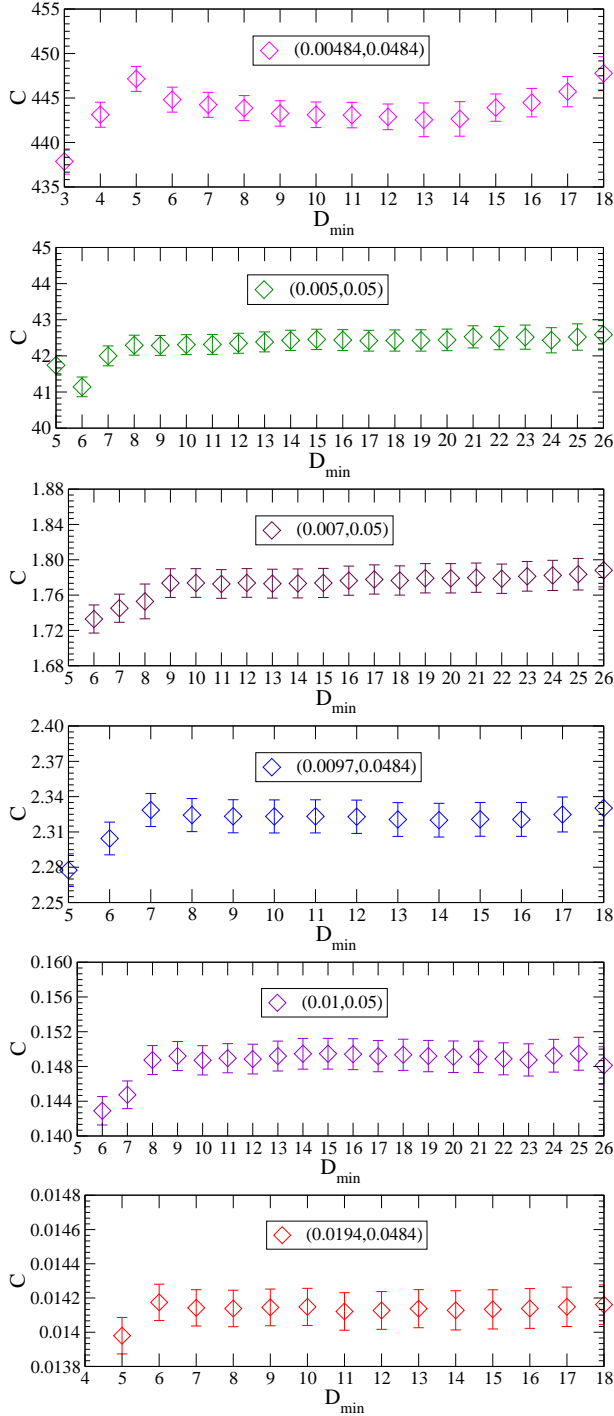


FIG. 8: (color online). The “effective wraparound constant” plots as the functions of  $D_{\min}$  for the  $\pi\pi$  scattering in the  $I = 2$  channel in lattice units.

Additionally, we clearly found that these fitted values of  $C$  are close to our estimated values listed in Table IV as already noticed in Ref. [30].

It is well-known that the interaction among two pions in the  $I = 2$  channel is pretty weak such that the energy difference between the interacting and non-interacting  $\pi\pi$

states is a quite small fraction of total energy of the  $\pi\pi$  system,<sup>8</sup> which can be estimated from the data in Tables II and V. This forces us to make the rigorous measurements of both the energies spectrum of the  $\pi\pi$  system and pion masses, and even seriously account for various small systematic effects to resolve the rather small differences. We have indeed extracted the energies of the  $\pi\pi$  system and pion masses with significantly high precision which are shown in Tables II and V.

Now it is straightforward to substitute these energies  $aE$  into Lüscher formula (6) and secure the relevant  $s$ -wave scattering lengths  $a_{\pi\pi}^{I=2}$ , where we plugged the pion masses in Column three in Table II. The center-of-mass scattering momentum  $k^2$  is computed by Eq. (5) with pion masses given in Table II. However, to get rid of the scale-setting uncertainties, it turns out to be more customary to adopt the dimensionless quantity:  $m_{\pi}a_{\pi\pi}^{I=2}$  [25, 26]. All of these values for each lattice ensemble are summarized in Table V, where the statistical errors of  $k^2$  are calculated from the statistical errors of  $aE$  and  $am_{\pi}$ , and its systematic errors are only estimated from the systematic errors of  $aE$ . Likewise, the statistical errors for  $m_{\pi}a_{\pi\pi}^{I=2}$  are computed from the systematic errors of  $k^2$  and  $am_{\pi}$ , while its systematic errors are estimated from the systematic errors of  $k^2$  and the subsequently-mentioned two finite volume effects.

Since the periodic boundary condition is imposed in the spacial directions of the lattice, there has an exponentially small finite volume (FV) correction to the  $s$ -wave  $\pi\pi$  scattering length in the  $I = 2$  channel, which has been determined in the vicinity of the threshold in Ref. [83]. The consequent finite volume correction  $\Delta_{FV}$  is provided here as [83],

$$(m_{\pi}a_{\pi\pi}^{I=2})_L = (m_{\pi}a_{\pi\pi}^{I=2})_{\infty} + \Delta_{FV} \quad (18)$$

where

$$\Delta_{FV} = \frac{1}{2^{13/2}\pi^{5/2}} \left(\frac{m_{\pi}}{f_{\pi}}\right)^4 \sum'_{\mathbf{n} \in \mathbb{Z}^3} \frac{e^{-|\mathbf{n}|m_{\pi}L}}{\sqrt{|\mathbf{n}|m_{\pi}L}} \times \left\{ 1 - \frac{17}{8} \frac{1}{|\mathbf{n}|m_{\pi}L} + \frac{169}{128} \frac{1}{|\mathbf{n}|^2 m_{\pi}^2 L^2} + \mathcal{O}(L^{-3}) \right\}, \quad (19)$$

here  $\sum'_{\mathbf{n} \in \mathbb{Z}^3}$  indicates a summation without  $\mathbf{n} = \mathbf{0}$ . Using this formula, we compute the finite volume corrections to  $m_{\pi}a_{\pi\pi}^{I=2}$ , which are listed in Table VI, where we insert the values of  $m_{\pi}L$  and  $m_{\pi}/f_{\pi}$  listed in Table II.

From Table VI, we note that these corrections are more and more important for the lattice ensembles with pion masses smaller and smaller [83]. Since we use the lattice ensembles with small pion masses, we should consider

<sup>8</sup> In this work, the ratio of the energy shift to total energy is about 2%. For other lattice studies [17–31], it is actually close to this number. On the other hand, this ratio for the  $I = 0$  channel is around 5% [18, 19, 32], and the ratio of this work is approximately to 5% as well.

TABLE V: Summaries of lattice results of the  $s$ -wave scattering lengths for the  $I = 2$  channel. The second block presents the energies in lattice units, where the first uncertainties are statistical, the second ones are the estimates of the systematic uncertainties due to fitting, Column three shows the fitted values of the wraparound term  $C$ , Column four indicates the time range for the chosen fit, and Column five gives the fit quality  $\chi^2/\text{dof}$ . Column seven gives the center-of-mass scattering momentum  $k^2$  in GeV, and Column eight presents the product of the pion mass and scattering length:  $m_\pi a_{\pi\pi}^{I=2}$ , where the first uncertainty is statistical and, the second one is systematic.

Ensemble	$aE$	$C$	Range	$\chi^2/\text{dof}$	$k^2[\text{GeV}^2]$	$m_\pi a_{\pi\pi}^{I=2}$
(0.00484, 0.0484)	0.35520(25)(20)	438.05(1.94)	14–24	4.21/6	0.00167(10)(7)	−0.0915(52)(35)
(0.005, 0.05)	0.32424(35)(33)	42.44(29)	16–32	10.6/12	0.00220(21)(15)	−0.125(11)(8)
(0.007, 0.05)	0.38606(44)(37)	1.776(17)	16–32	11.5/12	0.00444(31)(20)	−0.167(10)(7)
(0.0097, 0.0484)	0.50087(41)(38)	2.320(14)	14–24	6.1/6	0.00437(25)(17)	−0.167(9)(6)
(0.01, 0.05)	0.45648(56)(41)	0.1493(18)	18–32	8.7/10	0.00464(48)(26)	−0.209(19)(10)
(0.0194, 0.0484)	0.69392(40)(34)	0.01414(11)	13–24	6.6/7	0.00527(35)(22)	−0.277(16)(10)

TABLE VI: Summaries of the finite volume corrections  $\Delta_{\text{FV}}$ . Column two shows the finite volume corrections to the  $I = 2$   $\pi\pi$  scattering length, and Column three gives ratios of the finite volume corrections to the corresponding statistical error. Here we use the pion masses, pion decay constants and  $m_\pi L$  values listed in Table II.

Ensemble	$\Delta_{\text{FV}}$	Ratios
(0.00484, 0.0484)	0.000258	0.049
(0.005, 0.05)	0.000341	0.031
(0.007, 0.05)	0.000625	0.060
(0.0097, 0.0484)	0.000529	0.062
(0.01, 0.05)	0.000453	0.023
(0.0194, 0.0484)	0.000257	0.016

these effects, although they are slight, and never more than 7% of the corresponding statistical errors [27].

Another important finite volume effect stems from effective range approximation,  $k \cot \delta(k) = 1/a_{\pi\pi}^{I=2} + \frac{1}{2}rk^2$  [26]. While the dependence on the effective range  $r$  is small, and the range truncation actually leads to the correction at  $O(L^{-6})$  in Lüscher formula (6) [26]. In practice, we compute this correction for each lattice ensemble as suggested in Ref. [26].

These two finite volume corrections have been also added in quadrature to the systematic errors listed in Table V. Other sources of systematic uncertainty like: isospin violation, finite volume effect due to the fixed global topology, pion mass correction [26, 31], etc. are believed to be very small or we currently do not have enough computational resources to fulfil it. These effects should be incorporated into the more sophisticated lattice computation at some points in the future.

## B. $I = 0$ channel

As already performed for the  $I = 2$  channel, we analyze our lattice data with the “effective energy” plot. We

should stress that when using physical fitting model (14) to extract the desired energies  $aE$  of the  $\pi\pi$  system, we fix the fitting parameters of wraparound contribution  $C$  with the estimated values listed in Tables IV. <sup>9</sup> In practice, the  $\pi\pi$  four-point functions were fit by altering the minimum fitting distances  $D_{\text{min}}$ , and putting the maximum distance  $D_{\text{max}}$  either at  $T/2$  or where the fractional statistical errors exceeded about 20% for two sequential time slices [50, 61]. The “effective energy” plots as the functions of  $D_{\text{min}}$  are illustrated in Fig. 9. The central value and statistical error at each time slice were evaluated by Levenberg-Marquardt method [81]. To make these fits robust, we double-check them with SNOBFIT [82]. We do not show the result of (0.0194, 0.0484) ensemble in Fig. 9 since it is too noisy.

For each lattice ensemble, the energies  $aE$  of the  $\pi\pi$  system for the  $I = 0$  channel are secured from the “effective energy” plots, and chosen by looking for a combination of a “plateau” in the energy as the function of  $D_{\text{min}}$ , a good confidence level and  $D_{\text{min}}$  large enough to suppress the excited states [25–27]. In addition, as performed for isospin-2, we approximately estimate the systematic errors owing to fitting [25–27], which are not displayed in Fig. 9.

The fitted values of the energies  $aE$  of the  $\pi\pi$  system, fit range and fit quality ( $\chi^2/\text{dof}$ ) are summarized in Table VII. The fit quality  $\chi^2/\text{dof}$  is reasonable for the  $I = 0$  channel. It is well-known that the disconnected term give rise to the considerable fluctuations to the  $\pi\pi$  four-point function, and it is pretty hard to reliably calculate this term. In reality, only the lattice ensembles with small pion mass have a good signal. From Fig. 9, we found that, for the (0.097, 0.0484) and (0.01, 0.05) ensembles, the plateaus are not too obvious, so in this work, we don’t include these results.

<sup>9</sup> For rectangular (R), and vacuum (V) diagrams, there is no the wraparound pollution. So the wraparound contribution for the  $I = 0$  channel is the same with that in the  $I = 2$  channel. It is reasonable to fix the wraparound contribution  $C$ .

TABLE VII: Summaries of the lattice results for the fitted energies of the  $\pi\pi$  system for the  $I = 0$  channel. The second block shows the energies in lattice units, where the first uncertainties are statistical, the second ones are the estimates of the systematic uncertainties. Column three shows the fitting range, and Column four shows the number of degrees of freedom (dof) for the fit. The six block shows the center-of-mass scattering momentum  $k^2$  in GeV, and Column seven gives the product of pion mass and scattering length:  $m_\pi a_{\pi\pi}^{I=0}$ , where the first uncertainty is statistical and, the second one is systematic.

Ensemble	$aE$	Range	$\chi^2/\text{dof}$	$k^2[\text{GeV}^2]$	$m_\pi a_{\pi\pi}^{I=0}$
(0.00484, 0.0484)	0.33226(63)(78)	9 – 24	13.3/12	-0.00572(21)(24)	0.476(25)(29)
(0.005, 0.05)	0.3013(16)(18)	11 – 24	14.6/10	-0.00791(71)(76)	0.811(123)(133)
(0.007, 0.05)	0.3499(23)(26)	9 – 32	28.3/20	-0.0140(12)(13)	1.181(202)(223)

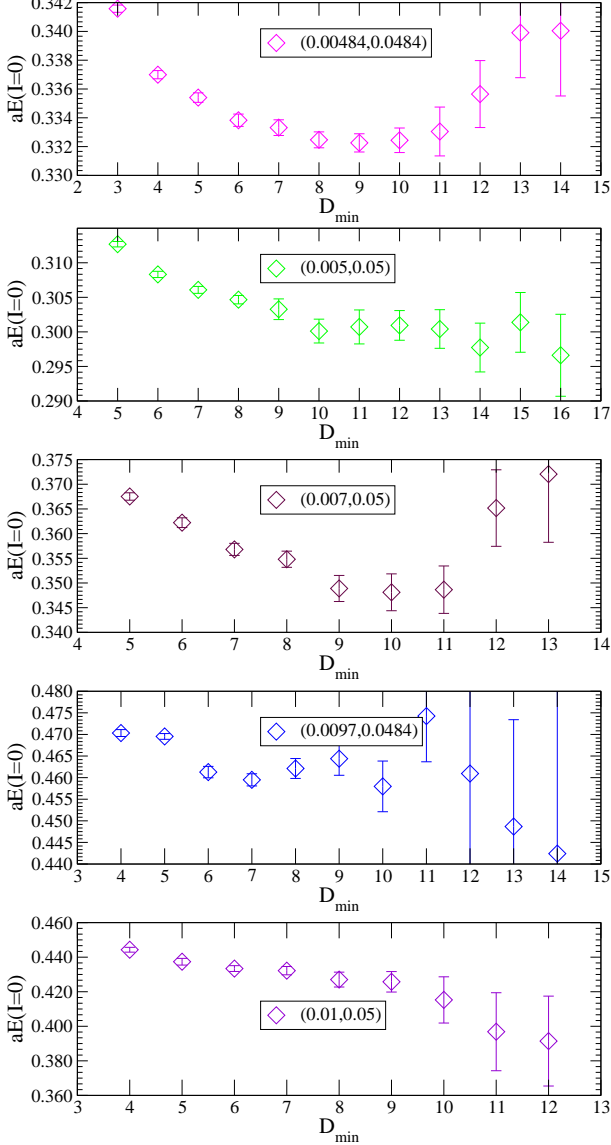


FIG. 9: (color online). The “effective energy” plots as the functions of  $D_{\min}$  for the  $\pi\pi$  scattering in the  $I = 0$  channel in lattice units.

Nevertheless, one thing greatly comforting us is that the interaction among two pions in this channel is not

too weak such that the discrete energies in a torus are shifted relatively bigger than that of the  $I = 2$  channel from the values relevant for noninteracting pions, and as we can see from Tables II and VII, the energy shift between the interacting and non-interacting  $\pi\pi$  states is not a too small fraction of total energy. This indicates that the rigorous calculation of disconnected diagrams is at present the most important thing.

The center-of-mass scattering momentum  $k^2$  is calculated by Eq. (5) with pion masses listed in Table II, and then the corresponding  $s$ -wave scattering lengths  $m_\pi a_{\pi\pi}^{I=0}$  can be obtained through Eq. (6). All of these values are summarized in Table VII, where the statistical errors of  $k^2$  are calculated from the statistical errors of the energies  $aE$  and pion mass  $am_\pi$ , and its systematic errors are only estimated from the systematic errors of  $aE$ . Likewise, the statistical for  $m_\pi a_{\pi\pi}^{I=0}$  are computed from the statistical errors of  $k^2$  and  $am_\pi$ , and its systematic errors are estimated from the systematic errors of  $k^2$  and one finite volume effect [27].

As already explained in the previous section, the dependence on the effective range  $r$  is small, and the range truncation actually leads to the finite volume correction at  $O(L^{-6})$  in Lüscher formula (6) [26]. In practice, we compute this correction for each lattice ensemble as suggested in Ref. [26]. This finite volume corrections have been combined in quadrature to the systematic errors listed in Table VII. Other sources of systematic uncertainty like: nonuniversal exponentially suppressed corrections[83], pion mass correction [26, 31, 83], etc. are believed to be very small as compared with the rather large systematic error of the energies  $aE$  or we currently do not have enough computational resources to fulfil it. With more reliable calculation of the energies  $aE$  of the  $\pi\pi$  system in the  $I = 0$  channel in the future, these effects should be eventually incorporated into the more sophisticated lattice computation.

We should point out that, in this work, we do not quote our results for the (0.01, 0.05), (0.097, 0.0484) and (0.0194, 0.0484) ensembles due to two considerations: First, the vacuum contributions of these ensembles are noisy (see Fig. 3), and it is pretty hard to see the clear plateau (see Fig. 9) in the “effective energy” plots. Second, the presence of the  $\sigma$  resonance is clearly presented in low energy [53, 84], and thus it should be necessary for

us to map out “avoided level crossings” between  $\sigma$  resonances and  $\pi\pi$  states with isospin-0 to secure the reliable scattering length as investigated in the  $\pi K$  scattering in Refs. [53, 84]. Luckily, as studied in Refs. [10, 53, 84], the contaminations from  $\sigma$  meson for three lattice ensembles with small pion masses are negligible. Therefore, we only consider these results in the rest of the analysis.

## VI. CHIRAL EXTRAPOLATIONS

In this work, we employed the rather small pion masses ranging from 240 MeV to 463 MeV, which are still larger than the physical one. Therefore,  $\chi$ PT is needed to carry out a chiral extrapolation of the scattering lengths to the physical pion mass. The resulting NLO  $\chi$ PT formulas, which can be directly built from the results in Ref. [2] (see Appendix A for details), are described as [27, 33]

$$m_\pi a_{\pi\pi}^{I=0} = \frac{7m_\pi^2}{16\pi f_\pi^2} \left\{ 1 - \frac{m_\pi^2}{16\pi^2 f_\pi^2} \times \left[ 9 \ln \frac{m_\pi^2}{f_\pi^2} - 5 - l_{\pi\pi}^{I=0}(\mu = f_{\pi,\text{phy}}) \right] \right\}, \quad (20)$$

$$m_\pi a_{\pi\pi}^{I=2} = -\frac{m_\pi^2}{8\pi f_\pi^2} \left\{ 1 + \frac{m_\pi^2}{16\pi^2 f_\pi^2} \times \left[ 3 \ln \frac{m_\pi^2}{f_\pi^2} - 1 - l_{\pi\pi}^{I=2}(\mu = f_{\pi,\text{phy}}) \right] \right\}, \quad (21)$$

where the values of  $m_\pi$  and  $f_\pi$  listed in Table II are inserted into, and the  $\chi$ PT renormalization scale is fixed at the physical pion decay constant  $\mu = f_{\pi,\text{phy}}$ . Where and whereafter a quantity with a “phys” subscript are referred to as the value of that quantity in the physical case. The  $l_{\pi\pi}^{I=0}(\mu)$  and  $l_{\pi\pi}^{I=2}(\mu)$  are the combinations of the LEC’s in  $\chi$ PT at a quark-mass independent scale  $\mu$  [25–27]. From the discussions in Appendix A, the  $l_{\pi\pi}^{I=0}(\mu)$  and  $l_{\pi\pi}^{I=2}(\mu)$  are connected to the LEC’s  $\bar{l}_n$  as [2, 85]

$$l_{\pi\pi}^{I=0} = \frac{40}{21}\bar{l}_1 + \frac{80}{21}\bar{l}_2 - \frac{5}{7}\bar{l}_3 + 4\bar{l}_4 + 9 \ln \frac{m_\pi^2}{f_{\pi,\text{phy}}^2}, \quad (22)$$

$$l_{\pi\pi}^{I=2} = \frac{8}{3}\bar{l}_1 + \frac{16}{3}\bar{l}_2 - \bar{l}_3 - 4\bar{l}_4 + 3 \ln \frac{m_\pi^2}{f_{\pi,\text{phy}}^2}. \quad (23)$$

It should be noted that the Eqs. (20) and (21) are expressed in terms of the full  $f_\pi$  computed on the lattice, and not the physical value  $f_{\pi,\text{phy}}$ . In reality, in the chiral expansion, the difference between utilizing  $f_\pi$  and  $f_{\pi,\text{phy}}$  in the argument of the logarithm only alters scattering lengths at higher orders [25, 26].

As recommended in Refs. [25–27], we will carry out the extrapolation of the products  $m_\pi a_{\pi\pi}^{I=2}$  and  $m_\pi a_{\pi\pi}^{I=0}$  by means of the ratio  $m_\pi/f_\pi$  in place of  $m_\pi$ . From Appendix A, we note that extrapolating in  $m_\pi/f_\pi$  in lieu of  $m_\pi$  does transform the representations for  $m_\pi a_{\pi\pi}^{I=2}$  and  $m_\pi a_{\pi\pi}^{I=0}$  but only at NNLO or higher. Additionally, since  $m_\pi/f_\pi$  is a dimensionless quantity, there is no systematic error arising from the scale setting [25–27].

We should remark that the lattice calculations reported here used two lattice spacing of 0.15 fm and 0.12 fm. Thus, it is meaningless to directly compare the energies  $aE$  of the  $\pi\pi$  system. However, on the assumption that the Lüscher technique properly explains for the finite volume dependence of the energies  $aE$  for these lattice ensembles, we can compare  $m_\pi a_{\pi\pi}^{I=2}$  and  $m_\pi a_{\pi\pi}^{I=0}$  for two lattice spacings [27], and we observe such agreement with statistical error in Table V.

### A. $I = 2$ channel

We are now in a position to fit lattice results of  $m_\pi a_{\pi\pi}^{I=2}$  in Table V to the NLO  $\chi$ PT functional form (21) to obtain low energy constant  $l_{\pi\pi}^{I=2}(\mu = f_{\pi,\text{phy}})$ , then the extrapolated value at the physical point  $(m_\pi a_{\pi\pi}^{I=2})_{\text{phys}}$  can be obtained. The lattice-calculated values of  $m_\pi a_{\pi\pi}^{I=2}$  as the function of  $m_\pi/f_\pi$  are shown in Fig. 10, and the outer error on the extrapolated result represents the systematic error and statistical error combined in quadrature. The one-loop  $\chi$ PT fit curve is displayed by the black solid line, and the red plus point indicates its physical  $s$ -wave scattering length:  $(m_\pi a_{\pi\pi}^{I=2})_{\text{phys}}$ , which is the chiral extrapolation of the  $m_\pi a_{\pi\pi}^{I=2}$  at the physical limit. In the same figure, we present the tree-level prediction as well. It is important to note that lattice data manifests pretty small displacement from the tree-level forecast. Additionally, we notice that our lattice results for  $m_\pi a_{\pi\pi}^{I=2}$  are in general agreement with the one-loop formula. In fact, the deviation of  $(m_\pi a_{\pi\pi}^{I=2})_{\text{phys}}$  from tree-level prediction is a natural aftermath of NLO  $\chi$ PT fitting [27].

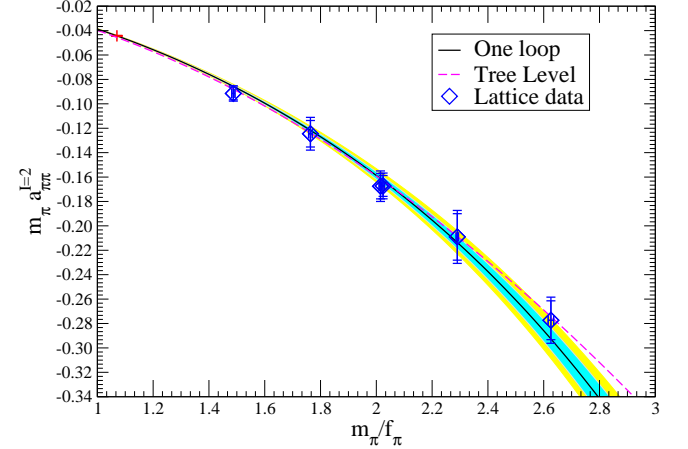


FIG. 10: (color online). The lattice-measured values of  $m_\pi a_{\pi\pi}^{I=2}$  as a function of  $m_\pi/f_\pi$ . The red plus point indicates the scattering length at the physical limit:  $(m_\pi a_{\pi\pi}^{I=2})_{\text{phys}}$ . The shaded bands correspond to statistical (inner-cyan) errors and statistical and systematic errors combined in quadrature (outer-yellow). The solid (black) curve is the central value of the NLO  $\chi$ PT fit. The dashed (magenta) line is the tree-level  $\chi$ PT prediction.

In principle, we can fit our lattice-calculated data to

TABLE VIII: A compilation of the various theoretical (or phenomenological), experimental and lattice QCD determinations of  $m_\pi a_{\pi\pi}^{I=2}$  extracted from the literature. Together with every reference, for an easier comparison, the first author name or the collaborations are given. The first uncertainty is statistical and second one is systematic if provided.

Ref.	$m_\pi a_{\pi\pi}^{I=2}$	Remarks
This work	$-0.04430 \pm 0.00025 \pm 0.00040$	The calculation made in this paper.
Yagi(2011) [31]	$-0.04410 \pm 0.00069 \pm 0.00018$	Extrapolation with NNLO $\chi$ PT.
Xu(2010) [27]	$-0.04385 \pm 0.00028 \pm 0.00038$	Using two flavors of maximally twisted mass fermions.
NPLQCD(2007) [26]	$-0.04330 \pm 0.00042$	Error combines statistical & systematic errors in quadrature.
CLQCD(2007) [20]	$-0.0399 \pm 0.0070$	The result from Scheme I of anisotropic lattices.
NPLQCD(2005) [25]	$-0.0426 \pm 0.0006 \pm 0.0003$	With fully-dynamical domain-wall valence-quark propagators.
Du(2004) [23]	$-0.0467 \pm 0.0045$	Using anisotropic lattices in an asymmetric box.
CP-PACS(2004) [24]	$-0.0413 \pm 0.0029$	Compensating the mass dependence of the scattering length.
JLQCD(2002) [22]	$-0.0410 \pm 0.0069$	Selecting the result from EXP which employs a single exponential.
Albaladejo(2012) [10]	$-0.0424 \pm 0.0012$	Employing unitary chiral perturbation theory.
Guo(2009) [9]	$-0.0444 \pm 0.0011$	Providing full results for all the contributing $\mathcal{O}(p^6)$ couplings.
Sasaki(2008) [8]	$-0.0431 \pm 0.0015$	Obtaining directly from the $\pi\pi$ wave function.
MILC(2004) [68]	$-0.0433 \pm 0.0009$	Using MILC's determinations of LECs along with Roy equations.
Zhou(2004) [7]	$-0.0440 \pm 0.0011$	Chiral unitarization with crossing symmetry & phase shift data.
CGL(2001) [3]	$-0.0444 \pm 0.0010$	Two loop accuracy.
Weinberg(1966) [1]	$-0.04557 \pm 0.00014$	Tree level prediction.
NA48/2(2011) [15, 16]	$-0.0429 \pm 0.0044 \pm 0.0016$	With independent experimental errors & different theoretical inputs.
E865(2003) [11]	$-0.0454 \pm 0.0031 \pm 0.0010$	With the $\chi$ PT constraints in the analysis.

the NNLO  $\chi$ PT form for  $m_\pi a_{\pi\pi}^{I=2}$  [2, 3] (see the concrete form in Eq. (A10)) as it is done in Ref. [31], since we have six lattice data at our disposal. In the meantime, we can make an estimate of NNLO LECs with the careful analysis for the chiral extrapolation of  $m_\pi a_{\pi\pi}^{I=2}$ , since we have lattice data points at the lighter quark masses. However, the NNLO fit has larger errors in both  $l_{\pi\pi}^{I=2}$  and  $m_\pi a_{\pi\pi}^{I=2}$  than those with NLO fit as shown in Refs. [25–27, 31], and the errors of the LECs  $l_{\pi\pi, I=2}^{(2)}$  and  $l_{\pi\pi, I=2}^{(3)}$  are rather large like the corresponding obtained values in Ref. [31]. Therefore, the calculations of NNLO LECs with physical meaning can not be obtained in this work. A rigorous NNLO  $\chi$ PT fit should wait for more lattice data at pion masses further closer to the physical point than we presently have. Admittedly, the resulting NNLO extrapolated value of  $m_\pi a_{\pi\pi}^{I=2}$  is indeed in harmony with NLO fit as we expect [27]. Actually, we use the NNLO  $\chi$ PT functional form to estimate systematic errors due to truncating the  $\chi$ PT series to NLO form [25].

As practiced in Ref. [27], we only consider three major sources of systematic uncertainty on the extrapolated value of  $m_\pi a_{\pi\pi}^{I=2}$  and  $l_{\pi\pi}^{I=2}$ . First, the lattice-calculated systematic errors of  $m_\pi a_{\pi\pi}^{I=2}$  per ensemble are spread by the chiral extrapolation [27]. Second, the systematic error inherently stems from NLO  $\chi$ PT fit [25, 26], which can be roughly calculated by taking the discrepancy between the NLO  $\chi$ PT extrapolated value from all six data sets and that from “pruning” the heaviest data set [27]. Third, the experimental errors on  $m_\pi$  and  $f_\pi$  [86] give rise to another important source of systematic er-

ror [27]. All three components are combined in quadrature to make up the entire systematic error. Taking the latest PDG data [86] for the most accurate charged pion mass  $m_\pi = m_{\pi^+} = 139.57018(35)$  MeV and pion decay constant  $f_\pi = f_{\pi^+} = 130.41(20)$  MeV, where a couple of experimental errors are added in quadrature, hence  $m_\pi/f_\pi = 1.07024(166)$ , we finally secure the upshots

$$\begin{aligned} m_\pi a_{\pi\pi}^{I=2} &= -0.04430(25)(40); \\ l_{\pi\pi}^{I=2}(\mu = f_{\pi, \text{phys}}) &= 3.27(.77)(1.12), \end{aligned} \quad (24)$$

where the first uncertainty is statistical and the second one is an estimate of the systematic error.

These outcomes are comparable with the aforementioned results of theoretical (or phenomenological) studies [1, 3, 7, 9, 10], experimental determinations [11, 15, 16] and lattice calculations [25–27, 31] within statistical errors. The relevant results for  $m_\pi a_{\pi\pi}^{I=2}$  are courteously compiled in Table VIII. The first group is lattice QCD results. The second one is theoretical (or phenomenological) studies. Also included are two experimental values in the third group.

To make our demonstrations of these results more intuitive, they are offered graphically in Fig. 11, where we clearly note that the various results for every  $m_\pi a_{\pi\pi}^{I=2}$  are fairly compatible with each other within errors.

Our calculation of the LEC  $l_{\pi\pi}^{I=2}$  is satisfactory as well, although it is just about 25% precision, while it can be comparable with relevant results obtained by phenomenological predictions [3], experimental determinations [11, 15, 16], and lattice calculations [25–27, 31].



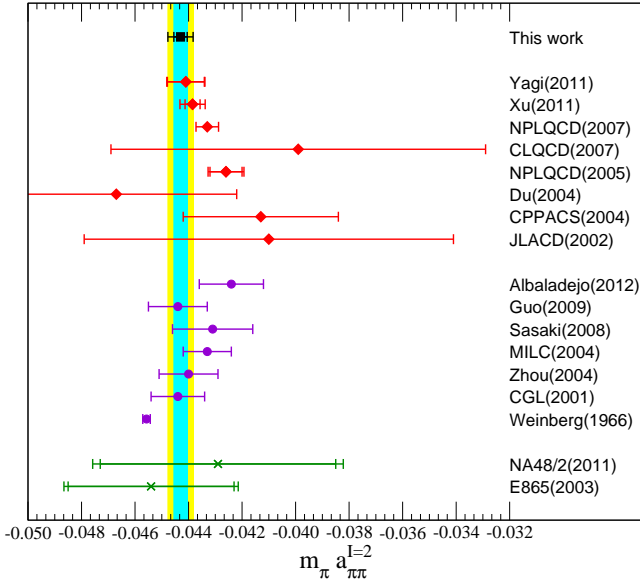


FIG. 11: (color online). A collection of various lattice QCD, theoretical (or phenomenological) and experimental results of  $m_\pi a_{\pi\pi}^{I=2}$  listed in Table VIII. The lattice studies are shown by red diamonds, purple circles are theoretical (or phenomenological) predictions, and the experimental ones are given by green crosses. Our result is indicated by a black square. For an easier comparison, the (cyan) inner strip corresponds to the statistical error whereas the (yellow) outer strip represents the statistical and systematic errors added in quadrature.

The relevant values of  $l_{\pi\pi}^{I=2}$  are collected in Table IX. The first group is lattice results. The second one is phenomenological and experimental determinations, which are transformed directly from the experimental and phenomenological results of  $m_\pi a_{\pi\pi}^{I=2}$  into  $l_{\pi\pi}^{I=2}$  at NLO  $\chi$ PT as preformed in Ref. [27].

The reason why we made a significant improvement in precision over our previous work [33] is the recent comprehension of various lattice-spacing artifacts (in particular wraparound effect). In fact, approximate 0.5% accuracy of our ultimate result for  $m_\pi a_{\pi\pi}^{I=2}$  is typically joint efforts from lattice QCD and  $\chi$ PT. This can be understood from two aspects: First, we have lattice data closer to the physical point, which have relatively smaller uncertainties for  $m_\pi a_{\pi\pi}^{I=2}$ . Second, the chiral extrapolation of  $m_\pi a_{\pi\pi}^{I=2}$  is considerably restricted by  $\chi$ PT and  $m_\pi a_{\pi\pi}^{I=2}$  is solely predicted in terms of  $m_\pi/f_\pi$  at LO and depends uniquely upon a LEC,  $l_{\pi\pi}^{I=2}$ , at NLO. This means that the statistical error of NLO  $\chi$ PT extrapolation of  $m_\pi a_{\pi\pi}^{I=2}$  solely rests on the statistical error of  $l_{\pi\pi}^{I=2}$ . Consequently, although our lattice-calculated results of  $m_\pi a_{\pi\pi}^{I=2}$  are only with about 6%  $\sim$  10% accuracy, we still obtain less than 1% precise determination of  $(m_\pi a_{\pi\pi}^{I=2})_{\text{phys}}$ .

TABLE IX: Some values of  $l_{\pi\pi}^{I=2}$  extracted from the literature. The first uncertainty is statistical, and the second one is systematic if present. The first group is lattice QCD results. The second one is phenomenological and experimental determinations, which are transformed directly from the corresponding results of  $m_\pi a_{\pi\pi}^{I=2}$  into  $l_{\pi\pi}^{I=2}$  at NLO  $\chi$ PT [27].

Ref.	$l_{\pi\pi}^{I=2}$
This work	$3.27 \pm 0.77 \pm 1.12$
Yagi(2011) [31]	$5.8 \pm 1.2$
Xu(2010) [27]	$4.65 \pm 0.85 \pm 1.07$
NPLQCD(2007) [26]	$6.2 \pm 1.2$
NPLQCD(2005) [25]	$3.3 \pm 0.6 \pm 0.3$
CGL(2001) [3]	$3.0 \pm 3.1^a$
NA48/2(2011) [15, 16]	$7.5 \pm 13.3 \pm 4.8^b$
E865(2003) [11]	$0.0 \pm 9.4 \pm 3.0$

<sup>a</sup> It is interesting to note that if we make use of Eq. (23) with the values of  $\bar{l}_i$  reported in Ref. [3], and necessary PDG values, we obtain  $l_{\pi\pi}^{I=2} = 2.0 \pm 3.1$ .

<sup>b</sup> Using the data from Ref. [15].

## B. $I = 0$ channel

We are now in a position for fitting lattice results of  $m_\pi a_{\pi\pi}^{I=0}$  in Table VII to NLO  $\chi$ PT functional form (20) to secure the low energy constant  $l_{\pi\pi}^{I=0}(\mu = f_{\pi,\text{phys}})$ , then obtain the extrapolated value at the physical point  $(m_\pi a_{\pi\pi}^{I=0})_{\text{phys}}$ . The lattice-measured values of  $m_\pi a_{\pi\pi}^{I=0}$  as the function of  $m_\pi/f_\pi$  are demonstrated in Fig. 12. The one-loop  $\chi$ PT fit curve is displayed by the black solid line, and the red circle point indicates its physical  $s$ -wave scattering length:  $(m_\pi a_{\pi\pi}^{I=0})_{\text{phys}}$ , which is the chiral extrapolation of the  $m_\pi a_{\pi\pi}^{I=0}$  at the physical point. In the same figure, we present the tree-level prediction as well. It is important to note that lattice data manifests a rather large displacement from the tree-level  $\chi$ PT forecast, which is well consistent with one conclusion of Ref. [3] that the NLO corrections make about 25% modification to tree-level prediction. Additionally, we can notice that our lattice results for  $m_\pi a_{\pi\pi}^{I=0}$  generally agree with the one-loop formula. The large deviation of  $(m_\pi a_{\pi\pi}^{I=0})_{\text{phys}}$  from tree-level prediction is totally a natural aftermath of the NLO  $\chi$ PT fitting.

In this work we can not fit our lattice-calculated data to the NNLO  $\chi$ PT functional form (20) [2, 3] (see concrete form (A10)), since we just have three lattice data at our disposal. A NNLO  $\chi$ PT determination should wait for more lattice data at pion masses further closer to the physical point than we now have. Admittedly, as explained in detail in Ref. [3], the NLO correction increases the LO prediction by about 25%, and NNLO correction further raises the LO prediction more than 10%, this mean that the NNLO  $\chi$ PT determination of  $m_\pi a_{\pi\pi}^{I=0}$  should be significantly more rigorous than the NLO  $\chi$ PT determination of  $(m_\pi a_{\pi\pi}^{I=0})_{\text{phys}}$ , and this can in part explain the relative large error for our final NLO

TABLE X: A compilation of the various theoretical (or phenomenological), experimental and lattice QCD determinations of  $m_\pi a_{\pi\pi}^{I=0}$  extracted from the literature. Together with every reference, for an easier comparison, the first author or the collaborations are given. The first uncertainty is statistical and the second one is systematic if given.

Ref.	$m_\pi a_{\pi\pi}^{I=0}$	Remark
This work	$0.214 \pm 0.004 \pm 0.007$	Full QCD.
Fu(2012) [33]	$0.186 \pm 0.002$	Partially quenched QCD.
Albaladejo(2012) [10]	$0.219 \pm 0.005$	Employing unitary chiral perturbation theory.
Guo(2009) [9]	$0.220 \pm 0.005$	Full results for all the contributing $\mathcal{O}(p^6)$ couplings.
Caprini(2008) [88]	$0.218 \pm 0.014$	Using a large class of analytic parameterizations.
Yndurain(2007) [87]	$0.233 \pm 0.013$	Extrapolating to the pole of the sigma resonance.
Zhou(2004) [7]	$0.211 \pm 0.011$	Using chiral unitarization with crossing symmetry & phase shift data.
CGL(2001) [3]	$0.220 \pm 0.005$	Two loop accuracy.
Weinberg(1966) [1]	$0.1595 \pm 0.0005$	Tree level prediction.
NA48/2(2011) [15, 16]	$0.2210 \pm 0.0047 \pm 0.0015$	With independent experimental errors & different theoretical inputs.
E865(2003) [11]	$0.216 \pm 0.013 \pm 0.002$	With the $\chi$ PT constraints in the analysis.

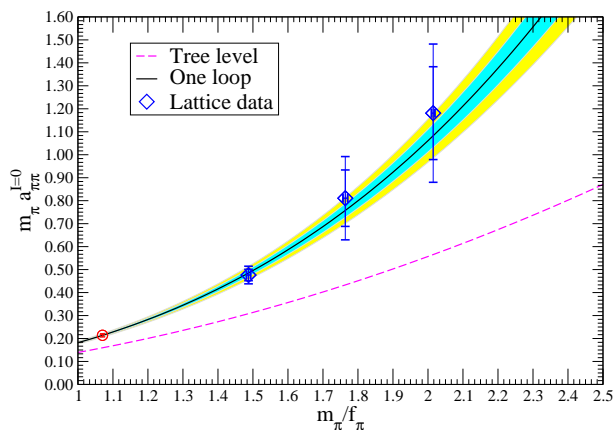


FIG. 12: (color online). The lattice-measured values of  $m_\pi a_{\pi\pi}^{I=0}$  as a function of  $m_\pi/f_\pi$ . The red circle point indicates the scattering length at the physical limit:  $(m_\pi a_{\pi\pi}^{I=0})_{\text{phys}}$ . The shaded bands correspond to statistical (inner-cyan) errors and statistical and systematic errors combined in quadrature (outer-yellow). The solid (black) curve is the central value of the NLO  $\chi$ PT fit. The dashed (magenta) line is the tree-level  $\chi$ PT prediction.

$\chi$ PT extrapolated result of  $(m_\pi a_{\pi\pi}^{I=0})_{\text{phys}}$ . As a consequence, the systematic error from truncating the  $\chi$ PT series to the NLO form should be considered.

In this work, we only consider two major sources of systematic errors in the extrapolated value of  $m_\pi a_{\pi\pi}^{I=0}$  since the systematic error from the experimental errors on  $m_\pi$  and  $f_\pi$  is found to be pretty small as compared with its statistical error. First, the lattice-computed systematic errors of  $m_\pi a_{\pi\pi}^{I=0}$  per ensemble are propagated via the chiral extrapolation. Second, the systematic error inherently stems from NLO fit, which is computed by taking the difference between the extrapolated values from NLO fit to all three data set and that from ‘cropping’ the heaviest data set [27]. All two parts are added

in quadrature to give the whole computed systematic error. We get the final upshot

$$\begin{aligned} m_\pi a_{\pi\pi}^{I=0} &= 0.214(4)(7); \\ l_{\pi\pi}^{I=0}(\mu = f_{\pi,\text{phys}}) &= 43.2 \pm 3.5 \pm 5.6, \end{aligned} \quad (25)$$

where the numbers in the first and second parentheses are the statistical and systematic uncertainty, respectively.

These results can be fairly comparable with the above-mentioned results by theoretical (or phenomenological) studies [1, 3, 7, 9, 10, 87, 88] (except the tree-level prediction), and experimental determinations [11, 15, 16]. The relevant results for  $m_\pi a_{\pi\pi}^{I=0}$  are compiled in Table X. The first group is lattice results. The second one is theoretical (or phenomenological) studies. Also contained are two experimental values in third group.

To make our report of these results more intuitive, these results are given graphically in Fig. 13 as well, where the various results of  $m_\pi a_{\pi\pi}^{I=0}$  are compatible with each other within errors except the tree-level prediction [1] and our crude lattice study [33].

Our calculation of the LEC  $l_{\pi\pi}^{I=0}$  is satisfactory as well, although it is about 5% accuracy, nevertheless, as we show soon, this result can be comparable with the results of phenomenological [3] and experimental determinations [11, 15, 16], and lattice studies [25–27, 31]. The relevant values of  $l_{\pi\pi}^{I=0}$  are collected in Table XI. The first group is lattice results. The second one is phenomenological and experimental determinations, which are converted directly from the experimental phenomenological results of  $m_\pi a_{\pi\pi}^{I=0}$  into  $l_{\pi\pi}^{I=0}$  at NLO  $\chi$ PT as conducted by Xu et al. in Ref. [27] for the  $I = 2$  channel.

The remarkable improvement in accuracy over our previous results [33] is a joint effort from lattice QCD and  $\chi$ PT. First, we have measured the lattice data closer to the physical point, which have smaller uncertainties. Second, chiral perturbation theory considerably constrains the chiral extrapolation of the product  $m_\pi a_{\pi\pi}^{I=0}$ , which is uniquely predicted in terms of  $m_\pi/f_\pi$  at LO and relies

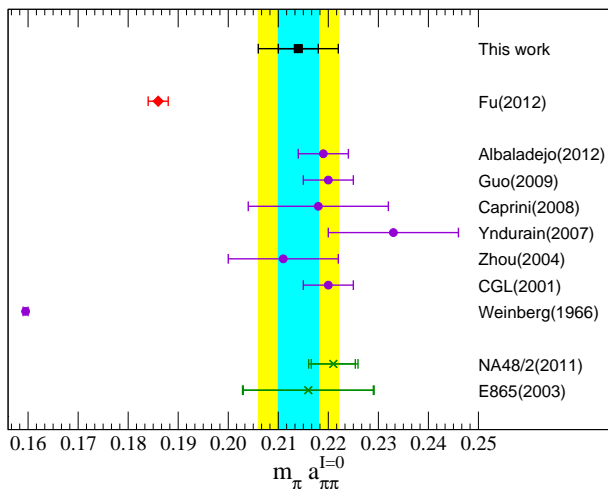


FIG. 13: (color online). A collection of various lattice QCD, theoretical (or phenomenological) and experimental results of  $m_\pi a_{\pi\pi}^{I=0}$  listed in Table X. The red diamonds are lattice determinations, purple circles are theoretical (or phenomenological) studies, and experimental ones are represented by green crosses. Our result is shown by a black square. For an easier comparison, the (cyan) inner strip corresponds to the statistical error whereas the (yellow) outer strip represents the statistical and systematic errors added in quadrature.

TABLE XI: Some values of  $l_{\pi\pi}^{I=0}$  extracted from the literature. The first uncertainty is statistical, and the second one is systematic if present. The first group is lattice simulation results. The second one is phenomenological and experimental determinations, which are directly transformed from the corresponding results of  $m_\pi a_{\pi\pi}^{I=0}$  into  $l_{\pi\pi}^{I=0}$  at NLO  $\chi$ PT [27].

	$l_{\pi\pi}^{I=0}$
This work	$43.2 \pm 3.5 \pm 5.6$
Fu(2012) [33]	$18.7 \pm 1.2$
CGL(2001) [3]	$48.5 \pm 4.3^a$
NA48/2(2011) [15]	$49.3 \pm 4.1 \pm 1.3$
E865(2003) [11]	$45.0 \pm 11.2 \pm 3.5$

<sup>a</sup> If we make use of Eq. (22) with the values of  $\bar{l}_i$  reported in Ref. [3], and required PDG values, we get  $l_{\pi\pi}^{I=0} = 32.4 \pm 2.3$ .

solely on a LEC,  $l_{\pi\pi}^{I=0}$ , at NLO. This suggests that the statistical error of NLO  $\chi$ PT extrapolation of  $m_\pi a_{\pi\pi}^{I=0}$  solely rests on the statistical error of  $l_{\pi\pi}^{I=0}$ . Consequently, although our lattice-calculated results of  $m_\pi a_{\pi\pi}^{I=0}$  are only with 5%  $\sim$  17% accuracy, we still obtain about 2% precise determination of  $(m_\pi a_{\pi\pi}^{I=0})_{\text{phys}}$ .

## VII. SUMMARY AND OUTLOOK

We have reported results of a lattice QCD calculation of the  $s$ -wave  $\pi\pi$  scattering lengths for both  $I = 0$  and 2 channels on the MILC “medium coarse” ( $a \approx 0.15$  fm) and “coarse” ( $a \approx 0.12$  fm) lattice ensembles with

the 2 + 1 flavors of the Asqtad-improved staggered sea quarks. We exploited the moving wall sources without the gauge fixing [18, 19] to compute all the four diagrams assorted in Refs. [17, 18], and viewed a clear attractive signal for the  $I = 0$  channel and a good repulsive one for the  $I = 2$  channel, respectively. Moreover, extrapolating our lattice data of the  $s$ -wave scattering lengths for both isospin eigenstates to the physical pion mass gives the scattering lengths:  $m_\pi a_{\pi\pi}^{I=2} = -0.04430(25)(40)$  and  $m_\pi a_{\pi\pi}^{I=0} = 0.214(4)(7)$  for the  $I = 2$  and 0 channels, respectively, which are in fair agreement with the current theoretical (or phenomenological) predictions to one-loop levels and the present experimental reports, and can be comparable with other lattice studies.

After our extremely crude estimation of the  $\pi\pi$  scattering length in the  $I = 0$  channel in Ref. [33], and this relatively more sophisticated computation, we can fairly claim that even with the limited computing resources, the lattice calculation of the  $\pi\pi$  scattering length in the  $I = 0$  channel is feasible although this work is absolutely needed to be further improved, and the various sources of systematic error yet need to be clarified thoroughly. Most of all, from this work, we found that the rule of thumb estimation of lattice ensemble with the Goldstone pion mass eligible to study the  $s$ -wave  $\pi\pi$  scattering in the  $I = 0$  channel should be less than about 300 MeV (the smaller, the better), which is very helpful for the people to pursue this fascinating enterprise. We view it as one of the important results of this work.

As we revealed, a reasonable signal can be gained for the (0.00484, 0.0484) and (0.005, 0.05) ensembles in the vacuum diagram of the  $\pi\pi$  scattering. In principle, the signal-to-noise ratio can be further enhanced by launching the same calculation on the lattice ensembles with a smaller pion mass (of course we can also improve the statistics by using more lattice gauge configurations or performing the calculation on a larger volume). In addition, the behavior close the physical point is intensely influenced by the chiral logarithm term, so an extraction of the  $\pi\pi$  scattering lengths without a long extrapolation is still highly needed to guarantee the convergence of the chiral expansion. Fortunately, the MILC collaboration has generated enough lattice ensembles whose Goldstone pion masses are smaller than or close to 240 MeV [89, 90] (e.g., the fine (0.00155, 0.0310) ensemble, whose Goldstone pion mass is about 177 MeV). Furthermore, as we explained early, the NNLO  $\chi$ PT will be the proper physical functional form to fit the lattice data (at least four data point) of the  $I = 0$   $\pi\pi$  scattering length and it needs more lattice data near the physical point. I have an impetus to do these works. However, it is beyond the scope of this work since this will need an astronomical amount of computing allocations. We will enthusiastically appeal for all the possible computational resources to accomplish this peculiar and challenging task.

It is well-known that  $\pi\pi$  scattering in the  $I = 0$  channel is challenging and stimulating phenomenologically due to the existence of the  $\sigma$  resonance. In the work, we have ex-

hibited that the  $\pi\pi$  scattering for the  $I = 0$  channel can be reliably calculated by the moving wall sources without gauge fixing [18, 19]. It gives us an anticipation that this technique can be successfully exploited to study the  $\sigma$  resonance. In our previous work [77], we have evaluated the  $\sigma$  mass from lattice QCD, and found that the decay  $\sigma \rightarrow \pi\pi$  is allowed kinematically only for enough small  $u$  quark mass. This work and our lattice calculation for the  $\pi\pi$  scattering lengths delivered in this paper will encourage the researchers to study the  $\sigma$  resonance. We have been investigating the  $\sigma$  resonance parameters with the isospin representation of  $(I, I_z) = (0, 0)$ , and the preliminary lattice results are already reported in Ref. [54].

Additionally, for  $\pi\pi$  scattering in the  $I = 0$  channel, we realize an important issue that the presence of  $\sigma$  resonance is possible in the low-energy, and thus it should be necessary for us to employ the variational method [38] to secure the rigorous scattering length as investigated in the  $\pi K$  scattering in the  $I = 1/2$  channel in Refs. [53, 84]. Since we only make use of the relative small quark masses to study the  $\pi\pi$  scattering in the  $I = 0$  channel, we can temporarily and reasonably overlook this contamination in the present study as already explained in Ref. [53]. However, we should bear in mind that this issue should be settled in the more sophisticated lattice examination. It will be very interesting to systematically study this pollution for the  $\pi\pi$  scattering in the  $I = 0$  channel.

Admittedly, due to the intense theoretical and experimental efforts put into the scalar-isoscalar and scalar-isovector sector of the meson-meson scattering recently, studying the  $K\bar{K}$  scattering length on the lattice is gradually becoming a very interesting enterprise. As pointed out in Ref. [91], the robust calculation of the  $\pi\pi$  scattering lengths (in particular for the  $I = 0$  channel) will naturally encourage us to study other challenging systems like  $K\bar{K}$ , etc. Physically, as explained in Ref. [60, 65, 92], studying  $K\bar{K}$  is very important, and the calculation of the  $s$ -wave  $K\bar{K}$  scattering length in the  $I = 0$  channel is a genuine two coupled-channel problem [65, 93], where the system can be approximately described by only  $\pi\pi$  and  $K\bar{K}$  two channels (we refer to  $\pi\pi$  as channel 1 and  $K\bar{K}$  channel 2), then the  $S$ -matrix is a  $2 \times 2$  unitary matrix which contains 3 real parameters [65, 93] (the  $s$ -wave  $K\bar{K}$  scattering in the  $I = 1$  channel can be treated analogously [59], and the lattice study of  $\pi\eta$  scattering is then highly desirable.). Therefore, it is absolutely necessary to incorporate the  $s$ -wave  $I = 0, \pi\pi$ -channel for a physical calculation of the  $s$ -wave  $K\bar{K}$  scattering length in the  $I = 0$  channel. The generalized Lüscher's formula in this case gives a relation among these three parameters, all of which are functions of the energy [93]. since some of these parameters are still poorly measured in the present experiments, the lattice calculation is valuable and highly desirable. With our lattice efforts on channel 2 in Ref. [60], at present, if we can compute the  $s$ -wave  $\pi\pi \rightarrow K\bar{K}$  scattering in the  $I = 0$  channel, in principle, we can solve this problem. We are launching a series of lattice studies for these aims.

## Acknowledgments

We feel indebted a lot to the MILC collaboration for using the Asqtad lattice ensembles and MILC codes. We should thank NERSC for providing us the platform to download MILC gauge configurations, and Dr. Massimo Di Pierro for his wonderful Python toolkit. The author profoundly thanks Carleton DeTar for indoctrinating me the necessary theoretical knowledge and computational skills for this work during my Ph.D study in University of Utah, and supplying us with the required software. The author deeply appreciates Paul Kienzle for teaching me computer skills during my work in NIST, Gaithersburg, USA. The author heartily thanks Grace Development Team for the use of xmgrace. We especially thank Eulogio Oset for his enlightening and constructive comments and corrections. The author must express my respect to Sasa Prelovsek and Liu chuan for reading this manuscript and giving some valuable comments. The author would like to express his gratitude to the Institute of Nuclear Science and Technology, Sichuan University where the computer resources and technical support are provided (in particular Hou Qing,<sup>10</sup> Zhu An, Ning Liu and Jun Wang). Numerical calculations for this paper were carried out at AMAX, CENTOS and HP workstations. Parts of numerical calculations were conducted at the Utah Center for High Performance Computing, University of Utah, during my Ph.D study.

## Appendix A: Scattering length of $\pi\pi$ in $\chi$ PT at NNLO

In Ref. [33], we provided the compact continuum three-flavor  $\chi$ PT form for the  $s$ -wave  $\pi\pi$  scattering length for isospin-0 at the NLO in the continuum limit of QCD by constructing from Appendix C in Ref. [2]. Here we follow the original derivations and notations in Refs. [2–4, 31] to derive its compact form at the NNLO.

The  $\pi\pi$  scattering lengths are provided at the NNLO of  $\chi$ PT in Refs. [2–4], and the  $s$ -wave  $\pi\pi$  scattering length in the  $I = 0$  channel is described as [2–4]

$$m_\pi a_{\pi\pi}^{I=0} = \frac{7m_\pi^2}{32\pi f_\pi^2} \left\{ 1 + \frac{x}{7} [49 + 5\bar{b}_1 + 12\bar{b}_2 + 48\bar{b}_3 + 32\bar{b}_4] + x^2 \left[ \frac{7045}{63} - \frac{215\pi^2}{126} + 10\bar{b}_1 + 24\bar{b}_2 + 96\bar{b}_3 + 64\bar{b}_4 + \frac{192}{7}\bar{b}_5 \right] \right\} + \mathcal{O}(x^4), \quad (\text{A1})$$

<sup>10</sup> The numerical calculations of this work are unceasingly carried out for more than two years. We should especially thank Prof. Hou qing's continuous encouragements and comprehensive support, without his kind and selfless help, it is not possible for us to launch this work, and have an opportunity to do it.

where  $x = m_\pi^2/(16\pi^2 f_\pi^2)$  is the chiral expansion parameter and  $\bar{b}_i$ 's are dimensionless combinations of the coupling constants introduced in Refs. [2, 3] to parameterize the pion scattering amplitude. After some strenuous algebraic manipulations, we can check that

$$\begin{aligned} 5\bar{b}_1 + 12\bar{b}_2 + 48\bar{b}_3 + 32\bar{b}_4 = & \frac{63}{2}\tilde{L} - \frac{503}{6}x\tilde{L}^2 \\ & - \frac{20}{3}\tilde{l}_1 + \frac{40}{3}\tilde{l}_2 - \frac{5}{2}\tilde{l}_3 + 14\tilde{l}_4 - \frac{63}{2} \\ & + x\tilde{L} \left( -\frac{388}{3}\tilde{l}_1 - \frac{472}{3}\tilde{l}_2 - 35\tilde{l}_3 + 154\tilde{l}_4 + \frac{1405}{12} \right) \\ & + x \left( \frac{80}{3}\tilde{l}_1\tilde{l}_4 + \frac{160}{3}\tilde{l}_2\tilde{l}_4 - 15\tilde{l}_3\tilde{l}_4 + 35\tilde{l}_4^2 - \frac{5}{2}\tilde{l}_3^2 \right. \\ & + \frac{364}{3}\tilde{l}_1 + \frac{1336}{9}\tilde{l}_2 + \frac{141}{4}\tilde{l}_3 - 126\tilde{l}_4 + \frac{162719}{432} \\ & \left. - \frac{373}{18}\pi^2 + 5\tilde{r}_1 + 12\tilde{r}_2 + 48\tilde{r}_3 + 32\tilde{r}_4 \right), \quad (\text{A2}) \end{aligned}$$

where the low-energy constants  $\tilde{l}_i$ ,  $\tilde{r}_i$  are the quark mass independent couplings from the subleading orders  $\mathcal{L}_4$ ,  $\mathcal{L}_6$  of the effective Lagrangian, respectively [3], and renormalized at the running scale  $\mu$ , and  $\tilde{L} = \ln(\mu^2/m_\pi^2)$ .

Inserting Eq. (A2) into Eq. (A1) and considering expression B. 3 of Ref. [3]

$$\begin{aligned} \bar{b}_5 = & \frac{85}{72}\tilde{L}^2 + \tilde{L} \left\{ \frac{7}{8}\tilde{l}_1 + \frac{107}{72}\tilde{l}_2 - \frac{625}{288} \right\} + \tilde{r}_5 \\ & + \frac{7}{54}\pi^2 - \frac{66029}{20736} + \mathcal{O}(x^4), \end{aligned}$$

we recast the result in the order of  $x$  as

$$\begin{aligned} m_\pi a_{\pi\pi}^{I=0} = & \frac{7m_\pi^2}{32\pi f_\pi^2} \left\{ 1 + \frac{x}{2} \left( 9\tilde{L} + l_a^0 \right) \right. \\ & \left. + x^2 \left( \frac{857}{42}\tilde{L}^2 + l_b^0\tilde{L} + l_c^0 \right) \right\} + \mathcal{O}(x^4), \quad (\text{A3}) \end{aligned}$$

with

$$\begin{aligned} l_a^0 = & \frac{40}{21}\tilde{l}_1 + \frac{80}{21}\tilde{l}_2 - \frac{5}{7}\tilde{l}_3 + 4\tilde{l}_4 + 5, \\ l_b^0 = & \frac{116}{21}\tilde{l}_1 + \frac{128}{7}\tilde{l}_2 - 5\tilde{l}_3 - 22\tilde{l}_4 - \frac{3595}{84}, \\ l_c^0 = & \frac{5}{7}\tilde{r}_1 + \frac{12}{7}\tilde{r}_2 + \frac{48}{7}\tilde{r}_3 + \frac{32}{7}\tilde{r}_4 + \frac{192}{7}\tilde{r}_5 \\ & + \frac{80}{21}\tilde{l}_1\tilde{l}_4 + \frac{160}{21}\tilde{l}_2\tilde{l}_4 - \frac{15}{7}\tilde{l}_3\tilde{l}_4 + 5\tilde{l}_4^2 \\ & - \frac{5}{14}\tilde{l}_3^2 + \frac{148}{21}\tilde{l}_1 + \frac{232}{21}\tilde{l}_2 + \frac{1}{28}\tilde{l}_3 \\ & + 10\tilde{l}_4 - \frac{17561}{504} + \frac{394}{63}\pi^2. \quad (\text{A4}) \end{aligned}$$

The right-hand side (rhs) of Eq. (A1) is scale independent [3]. On the whole, the rhs of Eq. (A3) is scale invariant as well. Therefore, in principle, we can select the running scale  $\mu$  stochastically. However, when fitting our lattice-obtained scattering lengths as a function of  $x$ , it is highly desired for us to settle the fitting parameters quark-mass independent. As it is done in Ref. [31], we select  $\mu = 4\pi f_{\pi,\text{phy}}$ . Using this scale, we can see

$$\tilde{L}(\mu = 4\pi f_{\pi,\text{phy}}) = -\ln x - 2x\tilde{l}_4(\mu = 4\pi f_{\pi,\text{phy}})$$

$$+ 2x \ln x + \mathcal{O}(x^2), \quad (\text{A5})$$

where we exploit the chiral expansion of the pion decay constant  $f_\pi = f_{\pi,\text{phy}}\{1 + x\tilde{l}_4 + \mathcal{O}(x^2)\}$  [3].

Plugging Eq. (A5) into Eq. (A3), and rearranging the result in the order of  $x$ , we achieve the  $\pi\pi$  scattering length in the  $I = 0$  channel as

$$\begin{aligned} m_\pi a_{\pi\pi}^{I=0} = & \frac{7m_\pi^2}{32\pi f_\pi^2} \left\{ 1 + \frac{m_\pi^2}{32\pi^2 f_\pi^2} \left[ -9 \ln \left( \frac{m_\pi^2}{16\pi^2 f_\pi^2} \right) + l_a^0 \right] \right. \\ & \left. + x^2 \left[ \frac{857}{42}(\ln x)^2 - (l_b^0 + 9) \ln x + (l_c^0 + 9\tilde{l}_4) \right] \right\} \\ & + \mathcal{O}(x^4). \quad (\text{A6}) \end{aligned}$$

The continuum  $\chi$ PT forms for the  $s$ -wave  $\pi\pi$  scattering length in the  $I = 2$  channel  $a_{\pi\pi}^{I=2}$  at the NNLO was presented by Yagi et. al. in Ref. [31], namely,

$$\begin{aligned} m_\pi a_{\pi\pi}^{I=2} = & -\frac{m_\pi^2}{16\pi f_\pi^2} \left\{ 1 + \frac{m_\pi^2}{32\pi^2 f_\pi^2} \left[ 3 \ln \left( \frac{m_\pi^2}{16\pi^2 f_\pi^2} \right) + l_a^2 \right] \right. \\ & \left. + x^2 \left[ -\frac{31}{6}(\ln x)^2 - (l_b^2 + 3) \ln x + (l_c^2 + 3\tilde{l}_4) \right] \right\} \\ & + \mathcal{O}(x^4). \quad (\text{A7}) \end{aligned}$$

with

$$\begin{aligned} l_a^2 = & -\frac{8}{3}\tilde{l}_1 - \frac{16}{3}\tilde{l}_2 + \tilde{l}_3 + 4\tilde{l}_4 - 1, \\ l_b^2 = & -\frac{4}{3}\tilde{l}_1 - 8\tilde{l}_2 + \tilde{l}_3 - 2\tilde{l}_4 + \frac{119}{12}, \\ l_c^2 = & \frac{1}{2}\tilde{l}_3^2 - \left( \frac{16}{3}\tilde{l}_1 + \frac{32}{3}\tilde{l}_2 - 3\tilde{l}_3 - 5\tilde{l}_4 \right) \tilde{l}_4 + \frac{4}{3}\tilde{l}_1 + \frac{16}{3}\tilde{l}_2 \\ & + \frac{7}{4}\tilde{l}_3 - 2\tilde{l}_4 + \frac{163}{16} - \frac{22}{9}\pi^2 - \tilde{r}_1 - 16\tilde{r}_4. \quad (\text{A8}) \end{aligned}$$

In the above equations,  $f_\pi$  is the pion decay constant, which is originally written as  $F_\pi$  (around 92.4 MeV) [2–4]. In the present work,  $\sqrt{2}F_\pi$  is denoted by  $f_\pi$  (about 130 MeV) for the convenience of the fitting our lattice data. Then the above equations are recast as

$$\begin{aligned} m_\pi a_{\pi\pi}^{I=0} = & \frac{7m_\pi^2}{16\pi f_\pi^2} \left\{ 1 - \frac{m_\pi^2}{16\pi^2 f_\pi^2} \left[ 9 \ln \frac{m_\pi^2}{f_\pi^2} - 5 - l_{\pi\pi}^{I=0} \right] \right. \\ & + \frac{m_\pi^4}{64\pi^2 f_\pi^4} \left[ \frac{857}{42} \left( \ln \frac{m_\pi^2}{f_\pi^2} \right)^2 \right. \\ & \left. \left. + l_{\pi\pi, I=0}^{(2)} \ln \frac{m_\pi^2}{f_\pi^2} + l_{\pi\pi, I=0}^{(3)} \right] \right\}, \quad (\text{A9}) \end{aligned}$$

$$\begin{aligned} m_\pi a_{\pi\pi}^{I=2} = & -\frac{m_\pi^2}{8\pi f_\pi^2} \left\{ 1 + \frac{m_\pi^2}{16\pi^2 f_\pi^2} \left[ 3 \ln \frac{m_\pi^2}{f_\pi^2} - 1 - l_{\pi\pi}^{I=2} \right] \right. \\ & + \frac{m_\pi^4}{64\pi^4 f_\pi^4} \left[ -\frac{31}{6} \left( \ln \frac{m_\pi^2}{f_\pi^2} \right)^2 \right. \\ & \left. \left. + l_{\pi\pi, I=2}^{(2)} \ln \frac{m_\pi^2}{f_\pi^2} + l_{\pi\pi, I=2}^{(3)} \right] \right\}, \quad (\text{A10}) \end{aligned}$$

where  $l_{\pi\pi}^{(i)}$ s are the combinations of LEC's in  $\chi$ PT at a quark-mass independent running scale since all the LEC's are independent of quark mass, therefore, we can regard them as the fitting parameters in the chiral extrapolation of the  $s$ -wave  $\pi\pi$  scattering lengths [31].

From Eqs. (A4), (A6), (A7) and (A8), we can easily get its specific forms of  $l_{\pi\pi}^{I=0}$  and  $l_{\pi\pi}^{I=2}$ , which are related to the Gasser-Leutwyler coefficients  $\bar{l}_i$  as [2, 85]

$$l_{\pi\pi}^{I=0} = \frac{40}{21}\bar{l}_1 + \frac{80}{21}\bar{l}_2 - \frac{5}{7}\bar{l}_3 + 4\bar{l}_4 + 9 \ln \frac{m_\pi^2}{f_{\pi,\text{phy}}^2}, \quad (\text{A11})$$

$$l_{\pi\pi}^{I=2} = \frac{8}{3}\bar{l}_1 + \frac{16}{3}\bar{l}_2 - \bar{l}_3 - 4\bar{l}_4 + 3 \ln \frac{m_\pi^2}{f_{\pi,\text{phy}}^2}. \quad (\text{A12})$$

where we consider the equality  $\bar{l}_n = \tilde{l}_n + \ln(m_\pi^2/\mu^2)$  [3].

These are the forms what we used in our previous work [33]. For the other  $l_{\pi\pi}^{(i)}$ s, its explicit forms are given or can be inferred from Eqs. (A4), (A6), (A7) and (A8). It is interesting and important to note that if we opt the running scale  $\mu = f_{\pi,\text{phy}}$ , we obtain the same expressions.

- 
- [1] S. Weinberg, Phys. Rev. Lett. **17**, 616 (1966).  
[2] J. Bijnens, G. Colangelo, G. Ecker, J. Gasser and M. E. Sainio, Nucl. Phys. B **508**, 263 (1997) [arXiv:hep-ph/9707291].  
[3] G. Colangelo, J. Gasser and H. Leutwyler, Nucl. Phys. B **603**, 125 (2001) [arXiv:hep-ph/0103088].  
[4] G. Colangelo, J. Gasser and H. Leutwyler, Phys. Lett. B **488**, 261 (2000) [hep-ph/0007112].  
[5] S. M. Roy, Phys. Lett. B **36**, 353 (1971).  
[6] B. Ananthanarayan, G. Colangelo, J. Gasser and H. Leutwyler, Phys. Rept. **353**, 207 (2001) [arXiv:hep-ph/0005297].  
[7] Z. Y. Zhou, G. Y. Qin, P. Zhang, Z. Xiao, H. Q. Zheng and N. Wu, JHEP **0502**, 043 (2005) [hep-ph/0406271].  
[8] K. Sasaki and N. Ishizuka, Phys. Rev. D **78**, 014511 (2008).  
[9] Z. H. Guo and J. J. Sanz-Cillero, Phys. Rev. D **79**, 096006 (2009) [arXiv:0903.0782 [hep-ph]].  
[10] M. Albaladejo and J. A. Oller, Phys. Rev. D **86**, 034003 (2012) [arXiv:1205.6606 [hep-ph]].  
[11] S. Pislak, R. Appel, G. S. Atoyan, B. Bassalleck, D. R. Bergman, N. Cheung, S. Dhawan and H. Do *et al.*, Phys. Rev. D **67**, 072004 (2003) [hep-ex/0301040].  
[12] R. Garcia-Martin, R. Kaminski, J. R. Pelaez, J. Ruiz de Elvira, F. J. Yndurain, Phys. Rev. D **83**, 074004 (2011) [arXiv:1102.2183 [hep-ph]].  
[13] J. R. Batley *et al.* [NA48/2 Collaboration], Eur. Phys. J. C **54**, 411 (2008).  
[14] J. R. Batley *et al.* [NA48-2 Collaboration], Eur. Phys. J. C **70**, 635 (2010).  
[15] A. Bizzeti, AIP Conf. Proc. **1374**, 639 (2011).  
[16] R. Wanke, Nucl. Phys. Proc. Suppl. **210-211**, 193 (2011).  
[17] S. R. Sharpe, R. Gupta and G. W. Kilcup, Nucl. Phys. B **383**, 309 (1992).  
[18] Y. Kuramashi, M. Fukugita, H. Mino, M. Okawa and A. Ukawa, Phys. Rev. Lett. **71** 2387 (1993).  
[19] M. Fukugita, Y. Kuramashi, M. Okawa, H. Mino and A. Ukawa, Phys. Rev. D **52**, 3003 (1995) [arXiv:hep-lat/9501024].  
[20] X. Li *et al.* [CLQCD Collaboration], JHEP **0706**, 053 (2007) [hep-lat/0703015].  
[21] R. Gupta, A. Patel and S. R. Sharpe, Phys. Rev. D **48**, 388 (1993) [arXiv:hep-lat/9301016].  
[22] S. Aoki *et al.* [JLQCD Collaboration], Phys. Rev. D **66**, 077501 (2002) [arXiv:hep-lat/0206011].  
[23] X. Du, G. W. Meng, C. Miao and C. Liu, Int. J. Mod. Phys. A **19**, 5609 (2004) [hep-lat/0404017].  
[24] T. Yamazaki *et al.* [CP-PACS Collaboration], Phys. Rev. D **70**, 074513 (2004) [arXiv:hep-lat/0402025].  
[25] S. R. Beane, P. R. Bedaque, K. Orginos and M. J. Savage, Phys. Rev. D **73**, 054503 (2006) [arXiv:hep-lat/0506013].  
[26] S. R. Beane, T. C. Luu, K. Orginos, A. Parreno, M. J. Savage, A. Torok and A. Walker-Loud, Phys. Rev. D **77**, 014505 (2008) [arXiv:0706.3026 [hep-lat]].  
[27] X. Feng, K. Jansen and D. B. Renner, Phys. Lett. B **684**, 268 (2010) [arXiv:0909.3255 [hep-lat]].  
[28] S. R. Beane *et al.* [NPLQCD Collaboration], Phys. Rev. D **85**, 034505 (2012) [arXiv:1107.5023 [hep-lat]].  
[29] J. J. Dudek, R. G. Edwards, M. J. Peardon, D. G. Richards and C. E. Thomas, Phys. Rev. D **83**, 071504 (2011) [arXiv:1011.6352 [hep-ph]].  
[30] J. J. Dudek, R. G. Edwards and C. E. Thomas, Phys. Rev. D **86**, 034031 (2012) [arXiv:1203.6041 [hep-ph]].  
[31] T. Yagi, S. Hashimoto, O. Morimatsu and M. Ohtani, arXiv:1108.2970 [hep-lat].  
[32] Q. Liu, PoS **LAT2009**, 101 (2009) [arXiv:0910.2658 [hep-lat]].  
[33] Z. Fu, Commun. Theor. Phys. **57**, 78 (2012) [arXiv:1110.3918 [hep-lat]].  
[34] G. P. Lepage, in Proceedings of TASI'89 Summer School, edited by T. DeGrand and D. Toussaint (World Scientific, Singapore, 1990), p. 97.  
[35] L. Maiani and M. Testa, Phys. Lett. B **245**, 585 (1990).  
[36] M. Lüscher, Commun. Math. Phys. **105** (1986) 153.  
[37] M. Lüscher, Nucl. Phys. B **354**, 531 (1991).  
[38] M. Luscher and U. Wolff, Nucl. Phys. B **339**, 222 (1990).  
[39] K. Rummukainen and S. A. Gottlieb, Nucl. Phys. B **450**, 397 (1995) [arXiv:hep-lat/9503028].  
[40] S. R. Beane, P. F. Bedaque, A. Parreño and M. J. Savage, Phys. Lett. B **585**, 106 (2004) [arXiv:hep-lat/0312004].  
[41] C. h. Kim, C. T. Sachrajda and S. R. Sharpe, Nucl. Phys. B **727**, 218 (2005) [arXiv:hep-lat/0507006].  
[42] N. H. Christ, C. Kim and T. Yamazaki, Phys. Rev. D **72**, 114506 (2005) [arXiv:hep-lat/0507009].  
[43] X. Feng, X. Li and C. Liu, Phys. Rev. D **70**, 014505 (2004) [hep-lat/0404001].  
[44] C. B. Lang, D. Mohler, S. Prelovsek, M. Vidmar, Phys. Rev. D **84**, 054503 (2011) [arXiv:1105.5636 [hep-lat]].  
[45] Z. Fu, Phys. Rev. D **85**, 014506 (2012) [arXiv:1110.0319 [hep-lat]].

- [46] L. Leskovec and S. Prelovsek, Phys. Rev. D **85**, 114507 (2012) [arXiv:1202.2145 [hep-lat]].
- [47] M. Doring, U. G. Meissner, E. Oset and A. Rusetsky, Eur. Phys. J. A **48**, 114 (2012) [arXiv:1205.4838 [hep-lat]].
- [48] R. A. Briceño and Z. Davoudi, arXiv:1212.3398 [hep-lat].
- [49] P. Guo, J. Dudek, R. Edwards and A. P. Szczepaniak, arXiv:1211.0929 [hep-lat].
- [50] C. W. Bernard *et al.*, Phys. Rev. D **64**, 054506 (2001) [arXiv:hep-lat/0104002].
- [51] C. Aubin *et al.*, Phys. Rev. D **70**, 094505 (2004) [arXiv:hep-lat/0402030].
- [52] K. Orginos and D. Toussaint, Phys. Rev. D **59**, 014501 (1998) [arXiv:hep-lat/9805009]; K. Orginos, D. Toussaint and R. L. Sugar, Phys. Rev. D **60**, 054503 (1999) [arXiv:hep-lat/9903032]; T. Blum *et al.*, Phys. Rev. D **55**, R1133 (1997) [arXiv:hep-lat/9609036]; J. F. Lagaë and D. K. Sinclair, Phys. Rev. D **59**, 014511 (1998) [arXiv:hep-lat/9806014]; G. P. Lepage, Phys. Rev. D **59**, 074502 (1999) [arXiv:hep-lat/9809157]; C. W. Bernard *et al.* [MILC Collaboration], Phys. Rev. D **61**, 111502(R) (2000) [arXiv:hep-lat/9912018].
- [53] Z. Fu, Phys. Rev. D **85**, 074501 (2012) [arXiv:1110.1422 [hep-lat]].
- [54] Z. Fu, JHEP **1207**, 142 (2012) [arXiv:1202.5834 [hep-lat]].
- [55] C. B. Lang, L. Leskovec, D. Mohler and S. Prelovsek, Phys. Rev. D **86**, 054508 (2012) [arXiv:1207.3204 [hep-lat]].
- [56] T. Blum *et al.*, Phys. Rev. D **84**, 114503 (2011) [arXiv:1106.2714 [hep-lat]].
- [57] Z. Fu, JHEP **1201**, 017 (2012) [arXiv:1110.5975 [hep-lat]].
- [58] Z. Fu and K. Fu, Phys. Rev. D **86**, 094507 (2012) [arXiv:1209.0350 [hep-lat]].
- [59] Z. Fu, Eur. Phys. J. C **72**, 2159 (2012) [arXiv:1201.3708 [hep-lat]].
- [60] Z. Fu, arXiv:1210.5185 [hep-lat].
- [61] T. DeGrand and C. E. Detar, *Lattice methods for quantum chromodynamics*, New Jersey, USA: World Scientific (2006) 345 p.
- [62] S. Dürr, C. Hoelbling and U. Wenger, Phys. Rev. D **70**, 094502 (2004); C. Bernard, Phys. Rev. D **73**, 114503 (2006); C. Bernard, M. Golterman, Y. Shamir and S. R. Sharpe, Phys. Lett. B **649**, 235 (2007); C. Bernard, M. Golterman and Y. Shamir, Phys. Rev. D **73**, 114511 (2006); M. Creutz, Phys. Lett. B **649**, 241 (2007); S. Dürr and C. Hoelbling, Phys. Rev. D **74**, 014513 (2006); A. Hasenfratz and R. Hoffmann, Phys. Rev. D **74**, 014511 (2006).
- [63] M. Albaladejo and J. A. Oller, Phys. Rev. Lett. **101**, 252002 (2008) [arXiv:0801.4929 [hep-ph]].
- [64] C. Hanhart, Phys. Lett. B **715**, 170 (2012) [arXiv:1203.6839 [hep-ph]].
- [65] M. Doring, U. -G. Meissner, E. Oset and A. Rusetsky, Eur. Phys. J. A **47**, 139 (2011) [arXiv:1107.3988 [hep-lat]].
- [66] D. Barkai, K. J. M. Moriarty and C. Rebbi, Phys. Lett. B **156**, 385 (1985); A. Mihaly, H. R. Fiebig, H. Markum and K. Rabitsch, Phys. Rev. D **55**, 3077 (1997); A. Mihály, Ph.D thesis, Lajos Kossuth University, Debrecen, 1998.
- [67] T. Umeda, Phys. Rev. D **75**, 094502 (2007) [arXiv:hep-lat/0701005].
- [68] C. Aubin *et al.* [MILC Collaboration], Phys. Rev. D **70**, 114501 (2004) [arXiv:hep-lat/0407028].
- [69] M. G. Alford, W. Dimm, G. P. Lepage, G. Hockney and P. B. Mackenzie, Phys. Lett. B **361**, 87 (1995) [arXiv:hep-lat/9507010].
- [70] A. Bazavov *et al.*, Rev. Mod. Phys. **82**, 1349 (2010) [arXiv:0903.3598 [hep-lat]].
- [71] D. B. Kaplan, Phys. Lett. B **288**, 342 (1992); Y. Shamir, Nucl. Phys. B **406**, 90 (1993); Y. Shamir, Phys. Rev. D **59**, 054506 (1999).
- [72] A. Hasenfratz and F. Knechtli, Phys. Rev. D **64**, 034504 (2001); T. A. DeGrand, A. Hasenfratz and T. G. Kovacs, Phys. Rev. D **67**, 054501 (2003); T. DeGrand, Phys. Rev. D **69**, 014504 (2004); S. Durr, C. Hoelbling and U. Wenger, Phys. Rev. D **70**, 094502 (2004).
- [73] D. B. Renner *et al.* [LHP Collaboration], Nucl. Phys. Proc. Suppl. **140**, 255 (2005); R. G. Edwards *et al.* [LHP Collaboration], PoS **LAT2005**, 056 (2006).
- [74] G. P. Lepage and P. B. Mackenzie, Phys. Rev. D **48**, 2250 (1993) [arXiv:hep-lat/9209022].
- [75] C. W. Bernard, T. Burch, K. Orginos, D. Toussaint, T. A. DeGrand, C. E. DeTar, S. A. Gottlieb and U. M. Heller *et al.*, Phys. Rev. D **62**, 034503 (2000) [hep-lat/0002028].
- [76] C. Bernard *et al.*, PoS **LAT2007**, 090 (2007) [arXiv:0710.1118 [hep-lat]].
- [77] Z. W. Fu, Chin. Phys. Lett. **28** (2011) 081202; Z. W. Fu and C. DeTar, Chin. Phys. C **35** 896 (2011); C. Bernard, C. E. DeTar, Z. Fu and S. Prelovsek, Phys. Rev. D **76**, 094504 (2007) [arXiv:0707.2402 [hep-lat]]; Z. Fu, 2006, UMI-32-34073 [arXiv:1103.1541 [hep-lat]].
- [78] J. Nagata, S. Muroya, A. Nakamura, Phys. Rev. C **80**, 045203 (2009) [arXiv:0812.1753 [hep-lat]].
- [79] S. Prelovsek, T. Draper, C. B. Lang, M. Limmer, K. -F. Liu, N. Mathur and D. Mohler, Phys. Rev. D **82**, 094507 (2010) [arXiv:1005.0948 [hep-lat]].
- [80] G. P. Lepage, B. Clark, C. T. H. Davies, K. Hornbostel, P. B. Mackenzie, C. Morningstar and H. Trotter, Nucl. Phys. Proc. Suppl. **106**, 12 (2002) [arXiv:hep-lat/0110175]; C. Morningstar, Nucl. Phys. Proc. Suppl. **109A**, 185 (2002) [arXiv:hep-lat/0112023]; M. Wingate, J. Shigemitsu, C. T. H. Davies, G. P. Lepage and H. D. Trotter,
- [81] W. H. Press, S. A. Teukolsky, W. T. Vetterling and B. P. Flannery, *Numerical recipes in C (2nd ed.): the art of scientific computing*, New York, NY, USA: Cambridge University Press, 1992.
- [82] W. Huyer and A. Neumaier, ACM Transactions on Mathematical Software (TOMS) Volume 35 Issue 2, (July 2008) Article No. 9; matlab implementation: <http://www.mat.univie.ac.at/~neum/software/snobfit/>; python: <http://reflectometry.org/danse/docs/snobfit/>.
- [83] P. F. Bedaque, I. Sato and A. Walker-Loud, Phys. Rev. D **73**, 074501 (2006) [arXiv:hep-lat/0601033].
- [84] K. Sasaki, N. Ishizuka, T. Yamazaki and M. Oka [PACS-CS Collaboration], Prog. Theor. Phys. Suppl. **186** (2010) 187.
- [85] J. Gasser and H. Leutwyler, Nucl. Phys. B **250**, 465 (1985).
- [86] J. Beringer *et al.* [Particle Data Group Collaboration], Phys. Rev. D **86**, 010001 (2012).
- [87] R. Garcia-Martin, J. R. Pelaez and F. J. Yndurain, Phys. Rev. D **76**, 074034 (2007) [hep-ph/0701025].
- [88] I. Caprini, Phys. Rev. D **77**, 114019 (2008)
- [89] G. Colangelo, S. Durr, A. Jüttner, L. Lellouch,

- H. Leutwyler, V. Lubicz, S. Necco and C. T. Sachrajda *et al.*, *Eur. Phys. J. C* **71**, 1695 (2011) [arXiv:1011.4408 [hep-lat]].
- [90] A. Bazavov *et al.* [MILC Collaboration], *PoS CD* **09**, 007 (2009) [arXiv:0910.2966 [hep-ph]].
- [91] M. J. Savage, *Prog. Part. Nucl. Phys.* **67**, 140 (2012) [arXiv:1110.5943 [nucl-th]].
- [92] J. A. Oller, E. Oset and J. R. Pelaez, *Phys. Rev. D* **59**, 074001 (1999) [hep-ph/9804209]; F. Guerrero and J. A. Oller, *Nucl. Phys. B* **537**, 459 (1999) [hep-ph/9805334].
- [93] S. He, X. Feng and C. Liu, *JHEP* **0507**, 011 (2005) [hep-lat/0504019]; M. Doring and U. G. Meissner, *JHEP* **1201**, 009 (2012) [arXiv:1111.0616 [hep-lat]]; M. T. Hansen and S. R. Sharpe, *Phys. Rev. D* **86**, 016007 (2012) [arXiv:1204.0826 [hep-lat]]; C. Liu, X. Feng and S. He, *Int. J. Mod. Phys. A* **21**, 847 (2006) [hep-lat/0508022]; N. Li and C. Liu, *Phys. Rev. D* **87**, 014502 (2013) [arXiv:1209.2201 [hep-lat]].